DIABETES

Decreased mitochondrial creatine kinase 2 impairs skeletal muscle mitochondrial function independently of insulin in type 2 diabetes

David Rizo-Roca[1]*, Dimitrius Santiago P. S. F. Guimarães[1], Logan A. Pendergrast[2], Nicolas Di Leo[1], Alexander V. Chibalin[2], Salwan Maqdasy[3], Mikael Rydén[3], Erik Näslund[4], Juleen R. Zierath[1,2], Anna Krook[1]*

Increased plasma creatine concentrations are associated with the risk of type 2 diabetes, but whether this alteration is associated with or causal for impairments in metabolism remains unexplored. Because skeletal muscle is the main disposal site of both creatine and glucose, we investigated the role of intramuscular creatine metabolism in the pathophysiology of insulin resistance in type 2 diabetes. In men with type 2 diabetes, plasma creatine concentrations were increased, and intramuscular phosphocreatine content was reduced. These alterations were coupled to reduced expression of sarcomeric mitochondrial creatine kinase 2 (*CKMT2*). In C57BL/6 mice fed a high-fat diet, neither supplementation with creatine for 2 weeks nor treatment with the creatine analog β-GPA for 1 week induced changes in glucose tolerance, suggesting that increased circulating creatine was associated with insulin resistance rather than causing it. In C2C12 myotubes, silencing *Ckmt2* using small interfering RNA reduced mitochondrial respiration, membrane potential, and glucose oxidation. Electroporation-mediated overexpression of *Ckmt2* in skeletal muscle of high-fat diet–fed male mice increased mitochondrial respiration, independent of creatine availability. Given that overexpression of *Ckmt2* improved mitochondrial function, we explored whether exercise regulates CKMT2 expression. Analysis of public data revealed that CKMT2 content was up-regulated by exercise training in both humans and mice. We reveal a previously underappreciated role of CKMT2 in mitochondrial homeostasis beyond its function for creatine phosphorylation, independent of insulin action. Collectively, our data provide functional evidence for how CKMT2 mediates mitochondrial dysfunction associated with type 2 diabetes.

INTRODUCTION

Insulin resistance associated with type 2 diabetes is characterized by alterations in energy metabolism. Because intracellular storage and transport of adenosine triphosphate (ATP) is limited, high-energy–demanding tissues, such as the brain and skeletal muscle, use creatine kinases to convert creatine into phosphocreatine as an energy buffer. Creatine can be both efficiently stored and transported across the cell membrane and is, therefore, an important energy shuttle. Thus, creatine metabolism can couple mitochondrial energy production with cytosolic energy demands (*1*).

Alterations in enzymes controlling creatine metabolism have emerged as multifaceted players in various pathophysiological contexts. For example, creatine metabolism mediates macrophage immune responses (*2*) and contributes to the metabolic rewiring observed in cancer cells (*3*). In white adipose tissue, impaired phosphocreatine metabolism contributes to the development of a proinflammatory environment, linking alteration in creatine metabolism to obesity and metabolic disease (*4*). Increased circulating amounts of creatine in plasma are associated with a higher risk of type 2 diabetes incidence in men (*5*). Thus, correlative evidence suggests that alterations in creatine metabolism may be involved in the development of metabolic dysfunction.

Perturbations in creatine metabolism stem from changes in the expression and activity of the creatine transporter and members of the creatine kinase family, proteins responsible for the membrane transport and interconversion of creatine into phosphocreatine. Creatine kinases exhibit tissue-specific and discrete intracellular localization (*6*). In the heart and skeletal muscle, the creatine kinase M-type isoenzyme is found in the cytosol, whereas the creatine kinase S-type [also known as sarcomeric mitochondrial creatine kinase 2 (sMtCK or CKMT2)] is located in the mitochondrial intermembrane space. CKMT2 exists as a homo-octamer, consisting of four dimers that serve as the stable structural units (*7*). CKMT2 functionally colocalizes with the adenine nucleotide translocator (ANT) to rapidly hydrolyze ATP into adenosine diphosphate (ADP) to phosphorylate creatine (*8*). Thus, given this tissue-specific distribution and intracellular localization, CKMT2 is a key regulator of oxidative phosphorylation (OXPHOS) and mitochondrial respiration in skeletal muscle (*9*). However, the precise role for this enzymatic machinery in skeletal muscle metabolism in type 2 diabetes is unexplored. Skeletal muscle is a primary tissue for both glucose (*10*) and creatine disposal (*11*) and, therefore, emerges as a crucial organ for investigating the role of creatine metabolism in the development of insulin resistance in type 2 diabetes. Here, we investigated whether creatine metabolism and CKMT2 content were altered in skeletal muscle from men with type 2 diabetes. We also determined how modulation of creatine metabolism affected metabolic health and mitochondrial function.

[1]Department of Physiology and Pharmacology, Karolinska Institutet, SE-171 77 Stockholm, Sweden. [2]Department of Molecular Medicine and Surgery, Karolinska Institutet, SE-171 77 Stockholm, Sweden. [3]Department of Medicine (H7), Karolinska Institutet, Karolinska University Hospital Huddinge, SE-141 86 Stockholm, Sweden. [4]Division of Surgery, Department of Clinical Sciences, Danderyd Hospital, Karolinska Institutet, SE-182 57 Danderyd, Stockholm, Sweden.
*Corresponding author. Email: david.rizo.roca@ki.se (D.R.-R.); anna.krook@ki.se (A.K.)

RESULTS

Skeletal muscle creatine metabolism is altered in men with type 2 diabetes and linked to aberrant glucose control

To determine whether creatine metabolism is perturbed in skeletal muscle in type 2 diabetes, we collected plasma samples and vastus lateralis muscle biopsies from men with normal glucose tolerance or with type 2 diabetes (fig. S1A). Clinical characteristics of the study participants are presented in Tables 1 and 2. We found that circulating fasting amounts of creatine were increased in plasma from men with type 2 diabetes (Fig. 1A) and were negatively correlated with the expression of the creatine transporter solute carrier family 6 member 8 (*SLC6A8*) in skeletal muscle (Fig. 1, B and C). Although the intramuscular content of creatine was higher in men with type 2 diabetes (Fig. 1D), phosphocreatine amounts were reduced (Fig. 1E), and these amounts were associated with the expression of *CKMT2* in skeletal muscle (Fig. 1, F and G). The intramuscular phosphocreatine amount was inversely correlated with fasting blood glucose, with opposing trends in men with type 2 diabetes as compared with men with normal glucose tolerance (Fig. 1H). Similarly, lower skeletal muscle *CKMT2* mRNA amounts were associated with higher post–oral glucose tolerance test (OGTT) circulating insulin in men with normal glucose tolerance (Fig. 1I) and higher hemoglobin A1c in men with type 2 diabetes (Fig. 1, I to J). *CKMT2* correlated positively with hip diameter in men with normal glucose tolerance, and it was associated with a larger waist-to-hip ratio in men with type 2 diabetes (Fig. 1I). The amounts of creatine precursors in plasma were largely unaltered (fig. S1, B to F), except for glycine, which was decreased in men with type 2 diabetes (fig. S1B). Given that body mass index (BMI) was higher in men with type 2 diabetes, we also examined whether BMI in itself explained the relationship between creatine metabolism and clinical features. Except for the positive correlation between BMI and amounts of plasma creatine (fig. S1G), BMI did not associate with either creatine/phosphocreatine or gene expression in skeletal muscle (fig. S1, H to K). Except for intracellular skeletal muscle creatine, comparisons between diagnosis groups remained significant after adjusting for BMI (fig. S1G: plasma creatine, $P = 0.04$; fig. S1H: intramuscular phosphocreatine, $P = 0.027$; fig. S1I: *CKMT2*, $P = 0.027$; and fig. S1J: *SLC6A8*, $P = 0.024$).

Glucose homeostasis is unaffected by changes in whole-body creatine amounts

We next investigated whether changes in circulating and skeletal muscle creatine/phosphocreatine amounts were associated with or directly impaired glucose homeostasis. We fed male C57BL/6 mice a high-fat diet for 8 weeks and then intraperitoneally injected phosphate-buffered saline (PBS), creatine, or the creatine analog

Table 1. Clinical characteristics of the individuals included in the metabolomic analysis. Results are means ± SEM for individuals with normal glucose tolerance ($n = 15$) and men with type 2 diabetes ($n = 25$). Statistical analysis was performed using Student's *t* test. FP-glucose, fasting plasma glucose; HOMA1-IR, homeostatic model assessment 1 for insulin resistance; P-ALAT, plasma alanine aminotransferase; P-ASAT, plasma aspartate aminotransferase; P-chol, plasma cholesterol; P-creatinine, plasma creatinine; P-HDL, plasma high-density lipoprotein cholesterol; P-LDL, plasma low-density lipoprotein cholesterol; P-TG, plasma triglyceride; S-insulin, serum insulin; WHR, waist-to-hip ratio.

	Normal glucose tolerance	Type 2 diabetes	*P* value
Age (years)	60 ± 2.4	63 ± 1.3	0.1339
Weight (kg)	82 ± 2.4	88 ± 1.8	0.0306
Height (m)	1.8 ± 0.02	1.79 ± 0.01	0.4615
BMI (kg/m^2)	25.95 ± 1.6	27.66 ± 0.47	0.0429
Waist (cm)	90 ± 1.6	100 ± 1.6	0.0003
Hip (cm)	97 ± 1.2	101 ± 1.2	0.0344
WHR	0.93 ± 0.01	0.99 ± 0.01	0.0009
Pulse (BPM)	62 ± 2.0	68 ± 1.6	0.0242
FP-glucose (mM)	5.41 ± 0.13	8.7 ± 0.37	<0.0001
120-min glucose (mM)	6.05 ± 0.25	16.78 ± 0.58	<0.0001
HbA1c (mmol/mol)	36.13 ± 1.13	51.19 ± 1.32	<0.0001
HbA1c (%)	5.5 ± 0.10	6.8 ± 0.12	<0.0001
S-insulin (pM)	52.37 ± 5.30	83.6 ± 9.20	0.0182
120 min S-insulin (pM)	294.2 ± 43.41	327.5 ± 42.06	0.6155
P-creatinine (μM)	84.53 ± 2.65	80.72 ± 2.17	0.1809
P-ASAT (μkat/liter)	0.42 ± 0.04	0.39 ± 0.03	0.6016
P-ALAT (μkat/liter)	0.38 ± 0.06	0.48 ± 0.04	0.1318
P-TG (mM)	1.08 ± 0.14	1.41 ± 0.13	0.0917
P-Chol (mM)	5.27 ± 0.17	4.50 ± 0.14	0.0014
P-HDL (mM)	1.33 ± 0.06	1.24 ± 0.06	0.3526
P-LDL (mM)	3.47 ± 0.13	2.62 ± 0.14	0.0004
S-C-peptide (nM)	0.69 ± 0.04	0.99 ± 0.08	0.0115
HOMA1-IR	1.71 ± 0.22	4.82 ± 0.65	0.0007

Table 2. Clinical characteristics of the individuals included in the transcriptomic analysis. Results are shown as means ± SEM for individuals with normal glucose tolerance ($n = 25$) and men with type 2 diabetes ($n = 22$). Statistical analysis was performed using Student's *t* test.

	Normal glucose tolerance	Type 2 diabetes	*P* value
Age (years)	58 ± 1.8	62 ± 1.3	0.0181
Weight (kg)	84 ± 1.7	89 ± 1.9	0.0577
Height (m)	1.80 ± 0.02	1.79 ± 0.01	0.6726
BMI (kg/m^2)	25.98 ± 0.35	27.94 ± 0.48	0.0044
Waist (cm)	93 ± 1.4	101 ± 1.7	0.0030
Hip (cm)	99 ± 0.9	101 ± 1.3	0.2420
WHR	0.94 ± 0.01	0.99 ± 0.01	0.0010
Pulse (BPM)	61 ± 1.4	68 ± 1.6	0.0064
FP-glucose (mM)	5.46 ± 0.08	8.56 ± 0.39	<0.0001
120-min glucose (mM)	5.89 ± 0.27	16.20 ± 0.69	<0.0001
HbA1c (mmol/mol)	35.76 ± 0.64	50.44 ± 1.50	<0.0001
HbA1c (%)	5.4 ± 0.06	6.8 ± 0.14	<0.0001
S-insulin (pM)	52.71 ± 5.58	92.58 ± 9.01	<0.0001
120-min S-insulin (pM)	314.9 ± 50.8	350.5 ± 42.4	0.6439
P-creatinine (μM)	83.64 ± 2.36	79.71 ± 2.29	0.1426
P-ASAT (μkat/liter)	0.38 ± 0.03	0.40 ± 0.03	0.7228
P-ALAT (μkat/liter)	0.42 ± 0.05	0.50 ± 0.04	0.3181
P-TG (mM)	1.25 ± 0.15	1.43 ± 0.13	0.2960
P-Chol (mM)	5.40 ± 0.20	4.48 ± 0.15	0.0018
P-HDL (mM)	1.30 ± 0.05	1.19 ± 0.06	0.1554
P-LDL (mM)	3.56 ± 0.17	2.63 ± 0.15	0.0008
S-C-peptide (mM)	0.69 ± 0.04	1.03 ± 0.08	0.0009
HOMA1-IR	1.86 ± 0.21	5.23 ± 0.65	<0.0001

β-guanidinopropionic acid (β-GPA; which acts as a competitive agonist to creatine for binding to the creatine transporter) for the last 2 weeks of the diet (Fig. 2A). As expected, high-fat diet–fed mice had increased body weight and fat mass and reduced lean body mass compared with those of chow-fed mice, with no differences between treatments (Fig. 2, B to D, and fig. S2, A to E). Similarly, fasting glucose and glucose tolerance were unaffected by either creatine or β-GPA administration in mice fed a high-fat diet (Fig. 2, E to G). Both basal and insulin-stimulated glucose transport in soleus muscle were decreased in high-fat diet–fed mice compared with chow diet–fed mice. Mice treated with β-GPA had improved basal glucose transport in soleus muscle and in insulin-stimulated glucose transport in extensor digitorum longus muscle (Fig. 2, H and I). Diet-induced insulin resistance and glucose intolerance were associated with skeletal muscle reduction in *Ckmt2* mRNA (Fig. 2J), recapitulating the results noted in people with type 2 diabetes. Compared with those in high-fat diet–fed mice treated with PBS, creatine treatment partially reverted the high-fat diet–induced down-regulation of *Ckmt2* mRNA (Fig. 2J) and up-regulated the expression of genes encoding antioxidant enzymes [catalase (*Cat*), nitric oxide synthase 1 (*Nos1*), nitric oxide synthase 3 (*Nos3*), and superoxide dismutase 1 (*Sod1*)], as well as hexokinase 2 (*Hk2*), pyruvate dehydrogenase kinase 4 (*Pdk4*), and vascular endothelial growth factor (*Vegf*) (Fig. 2K), although these changes were not all reflected by protein abundance (Fig. 2L).

Silencing of *Ckmt2* impairs mitochondrial homeostasis in C2C12 myotubes

Next, we assessed the pathophysiological consequences of experimental reduction of skeletal muscle *Ckmt2* expression. We silenced *Ckmt2* in C2C12 myotubes with small interfering RNA (siRNA), achieving a 60 to 90% knockdown at the mRNA level (Fig. 3A) and a reduction in protein abundance (Fig. 3B), each compared with that in a scrambled control. Mitochondrial respiration was assessed in intact C2C12 myotubes by high-resolution respirometry assays in an Oxygraph-2k (Fig. 3C). Compared with the scrambled control, *Ckmt2* silencing led to an overall decrease in mitochondrial respiration capacity, as evidenced by lower O_2 flux during basal oxygen consumption with glucose available in the medium and during the noncoupled state induced by carbonyl cyanide *p*-trifluoromethoxyphenylhydrazone (FCCP), to reveal the capacity of the electron transport chain (ETC) (Fig. 3D). The ratio between basal and uncoupled oxygen consumption (leak/ETC ratio) was increased in *Ckmt2*-silenced myotubes compared with that in scrambled siRNA–transfected controls (Fig. 3E). To assess whether impaired mitochondrial respiration was associated with changes in reactive oxygen species (ROS) production, we used fluorogenic dyes to measure superoxide (Fig. 3F) and hydrogen peroxide (Fig. 3G) production. Compared with scrambled siRNA transfection, *Ckmt2* silencing increased hydrogen peroxide in myotubes and decreased the mitochondrial membrane potential (Fig. 3H), as assessed by quantifying the mitochondrial potential dye tetramethylrhodamine

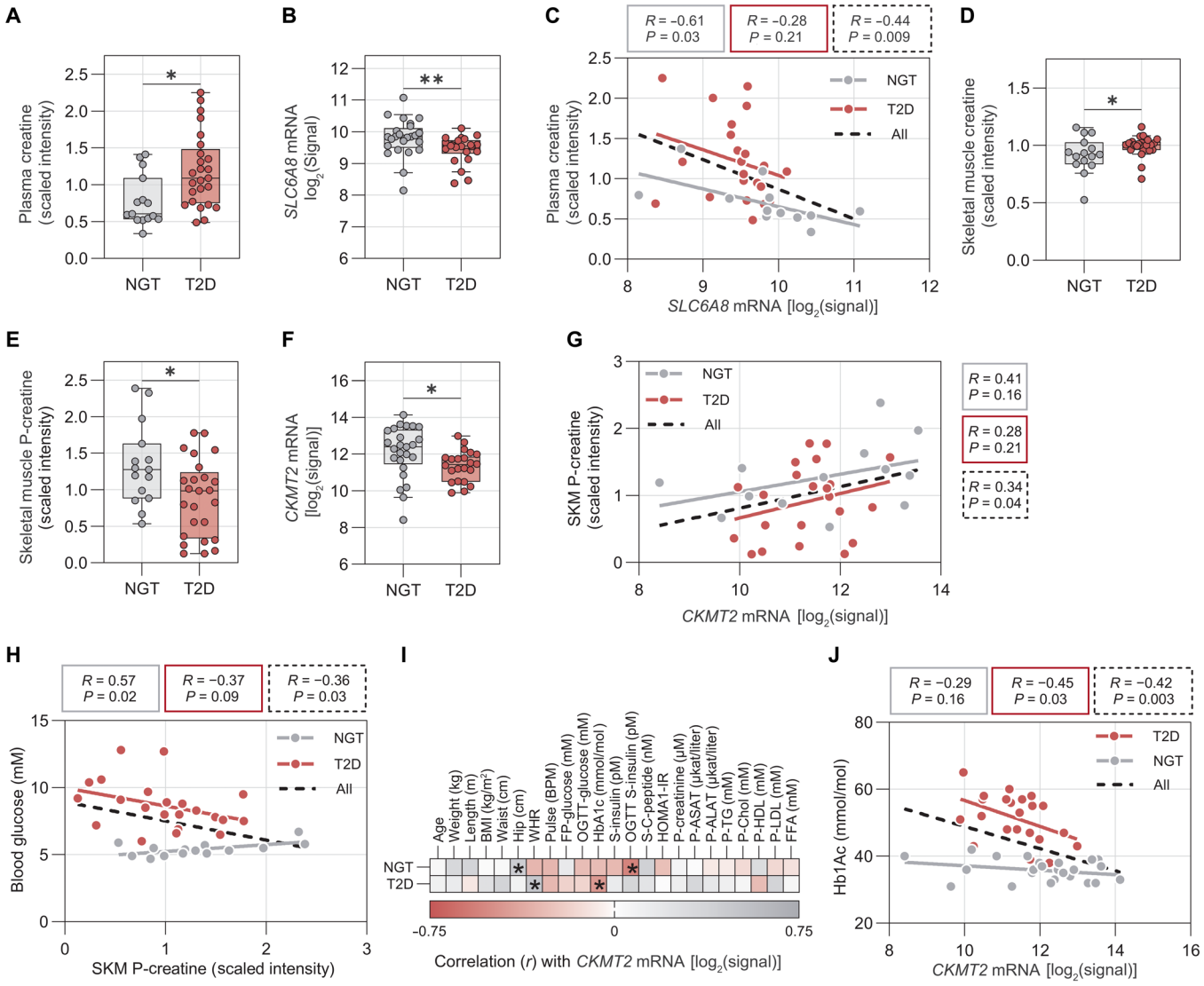

Fig. 1. SKM creatine metabolism is perturbed in men with type 2 diabetes and is linked to poorer glucose control. (**A**) Relative plasma creatine amounts from metabolomic analysis (peak intensity normalized to the median). Data are shown as a Tukey's boxplot. $n = 15$ in the normal glucose tolerance (NGT) group, and $n = 25$ in the type 2 diabetes (T2D) group. Statistical significance was determined by a two-tailed Mann-Whitney test. $^*P < 0.05$. (**B**) mRNA amounts of the creatine transporter gene *SLC6A8* from microarray. Data are shown as a Tukey's boxplot. $n = 25$ in the NGT group, and $n = 22$ in the T2D group. Statistical significance was determined by a two-tailed Mann-Whitney test. $^{**}P < 0.01$. (**C**) Pearson's correlation between *SLC6A8* mRNA amounts and plasma creatine relative peak intensity in a subset of individuals for whom both transcriptomic and metabolomic data were available (see fig. S1A). $n = 13$ in the NGT group, and $n = 22$ in the T2D group. (**D**) Relative skeletal muscle (SKM) creatine and (**E**) phosphocreatine amounts from metabolomic analysis (peak intensity normalized to the median). Data are shown as a Tukey's boxplot. $n = 15$ in the NGT group, and $n = 25$ in the T2D group. Statistical significance was determined by a two-tailed Mann-Whitney test (SKM creatine) or two-tailed Student's t test (SKM phosphocreatine). $^*P < 0.05$. (**F**) mRNA amounts of the sarcomeric mitochondrial creatine kinase gene *CKMT2* from microarray. Data are shown as a Tukey's boxplot. $n = 25$ in the NGT group, and $n = 22$ in the T2D group. Statistical significance was determined by a two-tailed Welch's t test. $^*P < 0.05$. (**G**) Pearson's correlation between *CKMT2* mRNA amounts and SKM phosphocreatine relative peak intensity in a subset of individuals for whom both transcriptomic and metabolomic data were available (see fig. S1A). (**H**) Pearson's correlation between SKM phosphocreatine amounts (peak intensity normalized to the median) and fasting blood glucose (millimolar). (**I**) Heatmap showing correlation between clinical characteristics and *CKMT2* mRNA amounts. Red is down-regulation, and gray is up-regulation. (**J**) Pearson's correlation between *CKMT2* mRNA amounts and Hb1Ac (millimoles per mole).

ethyl ester perchlorate (TMRE). Next, we incubated myotubes with D-[U-^{14}C]-glucose and ^{14}C-labeled CO_2 measured to assess glucose oxidation through the tricarboxylic acid cycle. Consistent with the decrease in mitochondrial respiration, we found that *Ckmt2* silencing reduced glucose oxidation compared with the scrambled control (Fig. 3I).

Citrate synthase enzymatic activity, a marker of mitochondrial content, and intracellular creatine content were unaltered (Fig. 3, J and K), suggesting that the attenuation in mitochondrial function and OXPHOS was caused by intrinsic functional or structural changes rather than a reduction in mitochondrial numbers or creatine availability. After analyzing electron microscopy micrographs

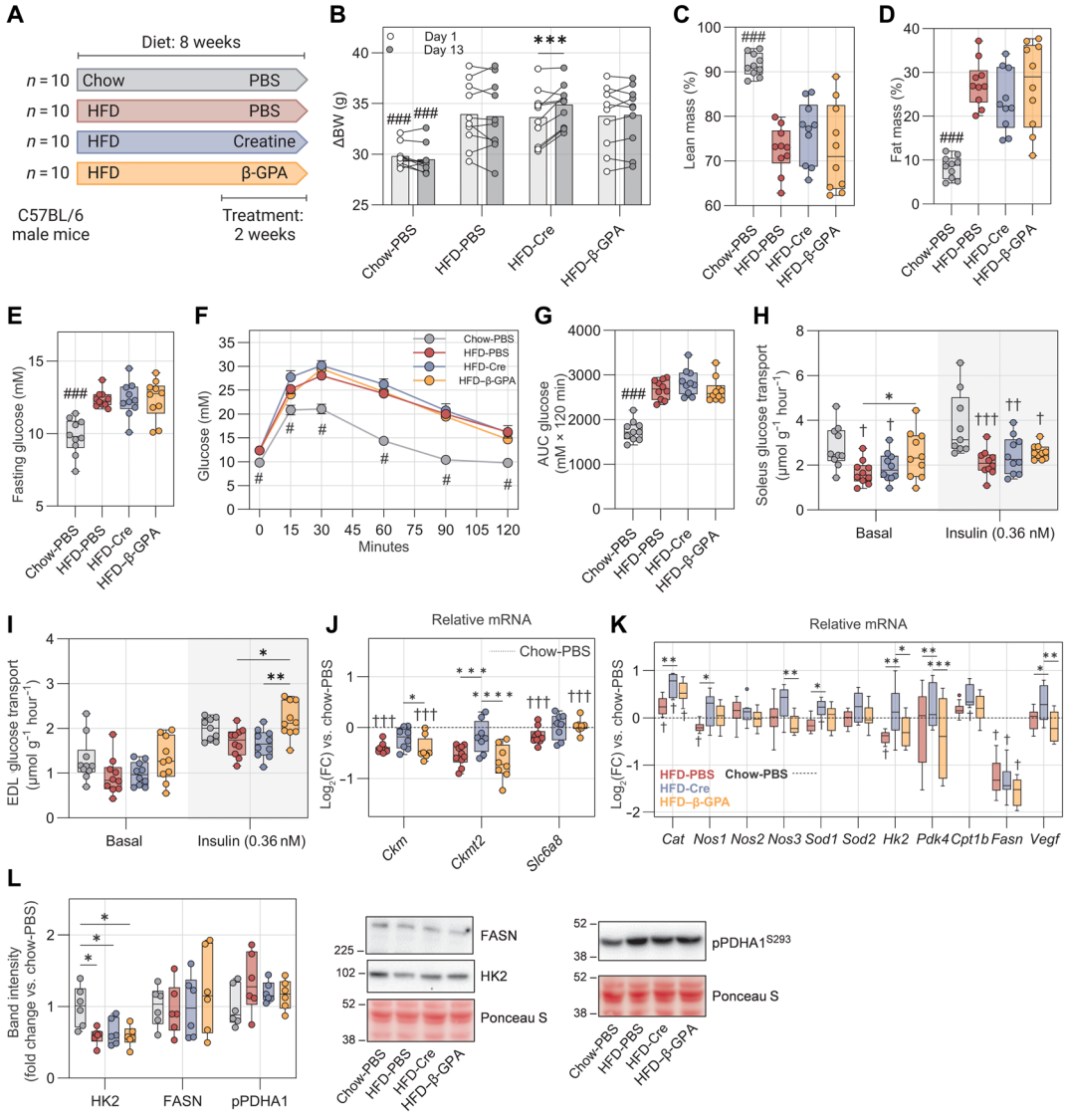

Fig. 2. Alterations in creatine availability do not modulate glucose metabolism in HFD–fed mice. (**A**) C57BL/6 male mice were fed with either a chow diet or a high-fat diet (HFD) for 8 weeks. For the last 2 weeks, mice were treated as follows: Mice fed with a chow diet were intraperitoneally injected daily with PBS, whereas mice fed with an HFD were intraperitoneally injected daily with PBS, creatine, or β-GPA. Experimental design created with BioRender.com. (**B**) Body weight (BW) before (sixth week of either chow diet or HFD) receiving the first intraperitoneal injection (day 1) and at intraperitoneal injection treatment day 13 (eighth week of either chow diet or HFD). Treatment is described in (A). Data are shown as means (bar) and individual values. $n = 10$ mice in each group. Statistical significance was determined by two independent two-way ANOVA (mixed-effects model) followed by Dunnett's post hoc test (HFD versus chow-PBS groups) or Tukey's post hoc test (when comparing the different treatments within the HFD-fed mice). ***$P < 0.001$. (**C**) Percentage of lean mass and (**D**) fat mass assessed by MRI at the end of the treatment [as described in (A)]. Data are shown as a Tukey's box plot. $n = 10$ mice in each group. Statistical significance was determined by two independent one-way ANOVA followed by Dunnett's post hoc test (HFD versus chow-PBS groups) or Tukey's post hoc test (when comparing the different treatments within the HFD-fed mice). ###$P < 0.001$ versus each HFD-fed group. (**E**) Fasting blood glucose (millimolar) after treatment [as described in (A)]. Data are shown as a Tukey's box plot. $n = 10$ mice in each group. Statistical significance was determined by two independent one-way ANOVA followed by Dunnett's post hoc test (HFD versus chow-PBS groups) or Tukey's post hoc test (when comparing the different treatments within the HFD-fed mice). ###$P < 0.001$ versus every HFD-fed group. (**F**) Time course of an intraperitoneal glucose tolerance test performed at the end of treatment [as described in (A)]. Data are presented as means ± SEM. $n = 10$ mice in each group. Statistical significance was determined by two independent two-way ANOVA (mixed-effects model) followed by Dunnett's post hoc test (HFD versus chow-PBS groups) or Tukey's post hoc test (when comparing the different treatments within the HFD-fed mice). #$P < 0.05$ versus each HFD-fed group. (**G**) Area under the curve (AUC) of the intraperitoneal glucose tolerance test. Data are shown as a Tukey's boxplot. $n = 10$ mice in each group. Statistical significance was determined by two independent one-way ANOVA followed by Dunnett's post hoc test (HFD versus chow-PBS groups) or Tukey's post hoc test (when comparing the different treatments within the HFD-fed mice). ###$P < 0.001$ versus each HFD-fed group. (**H**) Ex vivo soleus muscle and (**I**) extensor digitorum longus (EDL) muscle glucose transport (micromoles/gram per hour) in the absence (basal) or presence of 0.36 nM insulin in the incubation medium. Data are shown as a Tukey's boxplot. $n = 10$ mice in each group except in (H) chow-PBS (insulin), where $n = 9$. Two technical replicates were analyzed for each muscle, and the mean was used in the plot. Statistical significance was determined by two independent one-way ANOVA followed by Dunnett's post hoc test (HFD versus chow-PBS groups) or Tukey's post hoc test (when comparing the different treatments within the HFD-fed mice). *$P < 0.05$; **$P < 0.01$; †$P < 0.05$ versus chow-PBS; ††$P < 0.01$ versus chow-PBS; †††$P < 0.001$ versus chow-PBS. (**J**) Relative mRNA amounts of genes involved in creatine metabolism and in (**K**) antioxidant defense and metabolism in the tibialis anterior muscle. Data are shown as a Tukey's boxplot. $n = 10$ mice in the chow-PBS and HFD-PBS groups, and $n = 8$ in the HFD-Cre and HFD–β-GPA groups. qPCR was performed with technical duplicates. Statistical significance was determined by two independent one-way ANOVA followed by Dunnett's post hoc test (HFD versus chow-PBS groups) or Tukey's post hoc test (when comparing the different treatments within the HFD-fed mice). A Kruskal-Wallis test followed by Dunn's multiple comparisons test was applied in instances where data were not normally distributed [*Ckm* in (J) and *Cpt1b* in (K)]. *$P < 0.05$; **$P < 0.01$; ***$P < 0.001$; ****$P < 0.0001$; †$P < 0.05$ versus chow-PBS; †††$P < 0.001$ versus chow-PBS. FC, fold change. (**L**) Relative band intensity (left) and representative immunoblots of HK2, FASN (middle), and pPDHA1 proteins (right). Band intensity was normalized to Ponceau staining. Data are shown as a Tukey's boxplot. $n = 6$ mice in each group. Statistical significance was determined by two independent one-way ANOVA followed by Dunnett's post hoc test (HFD versus chow-PBS groups) or Tukey's post hoc test (when comparing the different treatments within the HFD-fed mice). *$P < 0.05$.

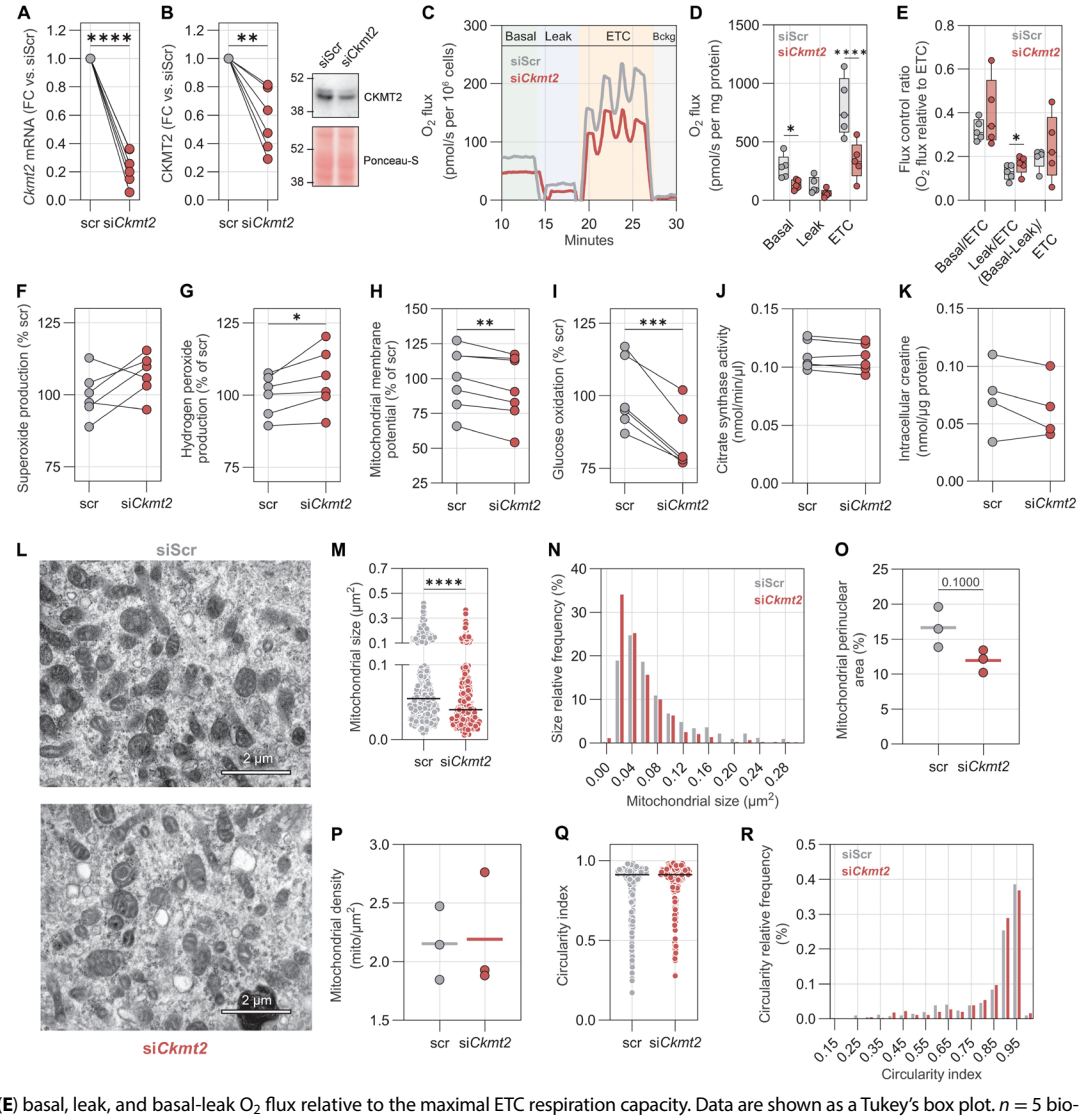

Fig. 3. Silencing of *Ckmt2* impairs mitochondrial homeostasis in myotubes. (**A**) Relative *Ckmt2* mRNA amounts after silencing in C2C12 myotubes. Data are shown as individual dots paired by passage. $n = 6$ biological replicates. Each biological replicate is a different passage. *Ckmt2*-silenced data were normalized to the scrambled control within each passage. qPCR was performed with technical duplicates. Statistical significance was determined by one-tailed paired Student's *t* test. $^{****}P < 0.0001$. (**B**) Relative band intensity (left) and representative immunoblot of CKMT2 (right) after *Ckmt2* silencing. Band intensity was normalized to Ponceau staining. Data are shown as individual dots paired by passage. $n = 6$ biological replicates. Each biological replicate is a different passage. *Ckmt2*-silenced data were normalized to the scrambled control within each passage. Statistical significance was determined by one-tailed paired Student's *t* test. $^{**}P < 0.01$. (**C**) Representative high-resolution respirometry assay conducted in intact C2C12 myotubes. The following compounds were added sequentially: oligomycin to assess leak respiration, FCCP titration to elicit maximal ETC respiration, and antimycin A to measure passive non-mitochondrial (background) oxygen consumption. Mitochondrial respiration in C2C12 myotubes in scrambled control and *Ckmt2*-silenced conditions was assessed by measuring (**D**) O_2 flux (picomoles per second per milligram of protein) during basal, leak, and ETC-fueled respiration states, and (**E**) basal, leak, and basal-leak O_2 flux relative to the maximal ETC respiration capacity. Data are shown as a Tukey's box plot. $n = 5$ biological replicates. Each biological replicate is a different passage. Statistical significance was determined by two-way ANOVA (repeated-measurements model) followed by Fisher's least significant difference (LSD) test. $^{*}P < 0.05$; $^{****}P < 0.0001$. (**F**) Relative changes in superoxide production, (**G**) hydrogen peroxide production, (**H**) mitochondrial membrane potential assessed by fluorimetry, and (**I**) ^{14}C-radiolabeled glucose oxidation rate in *Ckmt2*-silenced relative to scrambled control conditions. Data are shown as individual dots paired by passage. $n = 6$ biological replicates. Each biological replicate is a different passage. *Ckmt2*-silenced data were normalized to the scrambled control within each passage. Assays were conducted with technical duplicates. Statistical significance was determined by paired Student's *t* test. $^{*}P < 0.05$; $^{**}P < 0.01$; $^{***}P < 0.001$. (**J**) Citrate synthase activity (nanomoles per minute per microliter) assessed by enzymatic colorimetric assay in the *Ckmt2*-silenced condition compared with the scrambled control condition. Data are shown as individual dots paired by passage. $n = 6$ biological replicates. Each biological replicate is a different passage. The assay was conducted with technical duplicates. Statistical significance was determined by paired Student's *t* test. (**K**) Intracellular content of creatine (nanomoles per microgram of protein) measured by enzymatic colorimetric assay in scrambled control and *Ckmt2*-silenced conditions. Data are shown as individual dots paired by passage. $n = 4$ biological replicates. Each biological replicate is a different passage. The assay was conducted with technical duplicates. Statistical significance was determined by two-sided paired Student's *t* test. (**L**) Representative transmission electron microscopy images of C2C12 myotubes. Scale bars, 2 µm. (**M**) Differences between *Ckmt2*-silenced versus scrambled control conditions in mitochondrial morphology parameters are shown , including mitochondrial size (square micrometers). Data are shown as individual dots. The black line indicates the median. $n = 417$ mitochondria for the scrambled condition, and $n = 442$ mitochondria for the si*Ckmt2* condition. Mitochondria were analyzed and pooled from three different passages. Statistical significance was determined by a two-sided Mann-Whitney test. $^{****}P < 0.0001$. (**N**) The relative frequency distribution of sizes. Data are shown as a relative frequency histogram, indicating the percentage of mitochondria in each size range. $n = 417$ mitochondria for the scrambled condition, and $n = 442$ mitochondria for the si*Ckmt2* condition. (**O**) The percentage of nonnuclear analyzed area occupied by mitochondria. Data are shown as individual dots, and the lines indicate the mean. $n = 3$ biological replicates. Each biological replicate is a different passage. Statistical significance was determined by a two-sided Mann-Whitney test. (**P**) Mitochondrial density (number of mitochondria per square micrometer). Data are shown as individual dots, and the lines indicate the mean. $n = 3$ biological replicates. Each biological replicate is a different passage. Statistical significance was determined by a two-sided Mann-Whitney test. (**Q**) Mitochondrial circularity. Data are shown as individual dots. The black line indicates the median. $n = 417$ mitochondria for the scrambled condition, and $n = 442$ mitochondria for the si*Ckmt2* condition. Mitochondria were analyzed and pooled from three different passages. Statistical significance was determined by a two-sided Mann-Whitney test. (**R**) Relative frequency distribution of mitochondrial circularity. Data are shown as a relative frequency histogram, indicating the percentage of mitochondria in each circularity range. $n = 417$ mitochondria for the scrambled condition, and $n = 442$ mitochondria for the si*Ckmt2* condition.

(Fig. 3L), we found that, compared with the scrambled control, *Ckmt2* silencing resulted in smaller mitochondria, without altering the shape or number (Fig. 3, M to R).

Ckmt2 overexpression protects against lipid-induced metabolic stress in C2C12 myotubes independently of fatty acid handling

We next investigated whether *Ckmt2* overexpression protected against metabolic stress. C2C12 myotubes were transfected with a p*CMV-Ckmt2* plasmid and, 4 days later, cells were incubated for 24 hours with either vehicle or 0.5 mM of oleate and palmitate to induce insulin resistance (Fig. 4A). The p*CMV-Ckmt2* vector increased *Ckmt2* mRNA and protein expression (Fig. 4, B and C). Moreover, this expression remained elevated in oleate and palmitate–treated cells, whereas, under control conditions (empty vector), oleate and palmitate treatment down-regulated the expression of *Ckmt2* (Fig. 4D).

Overexpression of *Ckmt2* did not prevent the oleate and palmitate–induced down-regulation of peroxisome proliferator–activated receptor γ, coactivator 1 α (*Ppargc1a*) (Fig. 4E), suggesting that subsequent changes were not due to changes in the expression of this master regulator of mitochondrial function. Whereas we did not detect lipid-induced alterations in *Sod1* mRNA expression (Fig. 4F), *Ckmt2* overexpression prevented the decrease in *Sod2* mRNA induced by oleate and palmitate incubation (Fig. 4G) and up-regulated the expression of *Cat* (Fig. 4H). Consistently, p*CMV-Ckmt2*–transfected myotubes were resistant to oleate and palmitate–induced activation of the stress-responsive mitogen-activated protein kinase 14/p38 (MAPK14/p38), as reflected by lower relative amounts of T180/Y182 phosphorylation (Fig. 4I). This apparent protection against lipid-induced stress was not associated with changes in oxidation of either palmitate or glucose (Fig. 4, J to N, and fig. S3, A and B), suggesting that the benefits derived from *Ckmt2* overexpression may be related to structural, rather than metabolic changes. Similarly, intracellular creatine content remained unchanged between *Ckmt2* overexpression and the empty vector control (fig. S3C). Moreover, *Ckmt2* expression was particularly sensitive to oleate and palmitate incubation, resulting in a 55% reduction in mRNA amounts as compared with those in myotubes exposed to bovine serum albumin (BSA) (fig. S3D). Mammalian target of rapamycin signaling was unaffected by palmitate and oleate incubation and by *Ckmt2* overexpression (fig. S3, E to H).

Ckmt2 overexpression in skeletal muscle increases mitochondrial respiration and attenuates p38 MAPK activation in high-fat diet–fed mice

We next assessed the potential protective role of *Ckmt2* overexpression against lipid overload–induced metabolic stress. C57BL/6 male mice were fed a high-fat diet for 11 weeks, and the right and left tibialis anterior muscles were injected with p*CMV-Ckmt2* or an empty vector, respectively, followed by metabolic analysis 1 week later (Fig. 5, A to C). Mice were injected with ^{14}C-glucose and subjected to an OGTT, and, subsequently, skeletal muscle was removed. Compared to control muscles, overexpression of *Ckmt2* did not alter skeletal muscle glucose uptake (Fig. 5D) or phosphorylation of canonical proteins in the insulin-dependent signaling pathway such as AKT, AMP-activated protein kinase (AMPK), and acetyl–coenzyme A carboxylase (ACC) (Fig. 5E). In a separate experiment, permeabilized fiber bundles from electroporated tibialis anterior muscles were used to perform high-resolution respirometry assays (Fig. 5F). Compared with the control leg, *Ckmt2* overexpression increased complex I–driven mitochondrial respiration and complex I + II–driven maximal respiration (Fig. 5G), without altering the flux control ratio (oxygen consumption in a respiratory state normalized for the maximal respiration) (Fig. 5H). Protein abundance of the ETC subunits was not altered in skeletal muscles electroporated with the p*CMV-Ckmt2* vector (Fig. 5I). Moreover, tibialis anterior muscles electroporated with the p*CMV-Ckmt2* plasmid had reduced p38 MAPK and MAPK1/3/extracellular signal–regulated kinase 1/2 (Erk1/2) phosphorylation compared with the control leg (Fig. 5J).

CKMT2 content is increased by physical exercise

We next used publicly available datasets (ProteomeXchange Consortium PRIDE repository, accession codes PXD016289 and PXD026219; NCBI BioProject, accession code PRJNA732106) (*12*–*14*) to examine whether CKMT2 content is modulated by physical exercise. First, we found that 25 days of voluntary wheel running increased the content of CKMT2 in mitochondrial supercomplexes isolated from female C57BL/6JBomTac mice (PXD016289) (Fig. 6A) (*12*). Mitochondrial supercomplexes were composed, on average, of 200 different proteins, but only 2 to 12% were up-regulated by exercise (Fig. 6A, pie charts). Among these, CKMT2 was significantly increased in 7 of the 10 analyzed mitochondrial supercomplex compositions (Fig. 6A; supercomplex composition #1, $P = 0.004$; #2, $P = 0.007$; # 3, $P = 0.0005$; #5, $P = 0.02$; #6, $P = 0.002$; #7, $P = 0.041$; and #8, $P = 0.017$). These changes showed that wheel running specifically enriched CKMT2 in supercomplexes independently of mitochondrial biogenesis, because the same amount of mitochondrial protein was loaded in each lane.

A transcriptomic meta-analysis of *CKMT2* expression in studies of acute exercise, inactivity, and training in human trials was next obtained from the online database of skeletal muscle transcriptomic response to exercise (MetaMEx) (*13*). The meta-analysis performed by MetaMEx, including 70 human studies and 1420 skeletal muscle biopsies, revealed that *CKMT2* was up-regulated by acute high-intensity interval exercise and by aerobic and high-intensity interval training in metabolically healthy individuals (Fig. 6B). Conversely, physical inactivity (bed rest and unloading) was associated with a significant ($P = 1.4 \times 10^{-11}$) down-regulation of *CKMT2* (Fig. 6B). Individuals with insulin resistance exhibited a dampened response to exercise, and only training protocols combining aerobic and resistance exercise up-regulated *CKMT2* expression (Fig. 6B). In line with these results, our analysis of publicly available RNA sequencing (RNA-seq) (PRJNA732106) and proteomic datasets (PXD026219) (*14*) demonstrated not only that *CKMT2* mRNA was up-regulated after different exercise intensities (Fig. 6C) but also that exercise training increased CKMT2 protein abundance in mitochondria (Fig. 6D).

DISCUSSION

Here, we provide evidence linking type 2 diabetes to specific alterations in skeletal muscle creatine metabolism. Our findings indicate that elevated plasma creatine and reduced skeletal muscle phosphocreatine are markers, rather than drivers, of peripheral insulin resistance. Furthermore, we elucidate the role of skeletal muscle CKMT2 in mitochondrial homeostasis in type 2 diabetes. Increased plasma concentrations of creatine are linked to the risk of developing type 2 diabetes (*5*, *15*). Concordantly, we observed increased amounts of

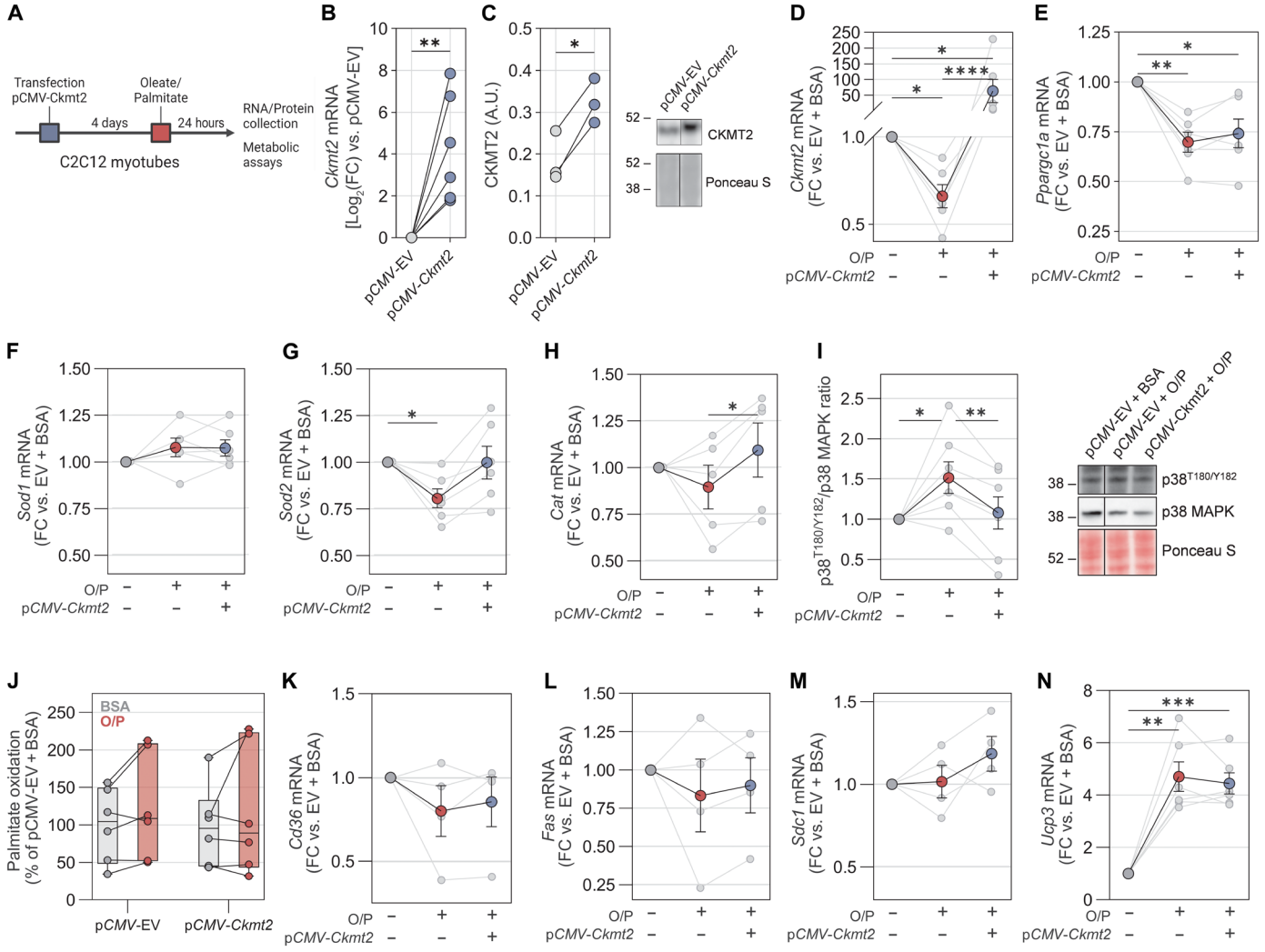

Fig. 4. Overexpression of *Ckmt2* protects against lipid overload–induced metabolic stress. (**A**) C2C12 myotubes were transfected with p*CMV-Ckmt2* vector and 4 days later incubated with 0.5 mM oleate and palmitate for 24 hours before performing the experiments. Schematic of the experimental design created with BioRender.com. (**B**) p*CMV*-mediated *Ckmt2* overexpression in C2C12 myotubes. Data are shown as individual dots paired by passage. $n = 6$ biological replicates. Each biological replicate is a different passage. Data were normalized to the empty vector (EV) incubated with BSA control within each passage. qPCR was performed with technical duplicates. Statistical significance was determined by one-tailed paired Student's *t* test. $^{**}P < 0.01$. (**C**) Representative immunoblot of CKMT2. A.U., arbitrary units. (**D**) mRNA amounts normalized to control cells of *Ckmt2*, (**E**) *Ppargc1a*, (**F**) *Sod1*, (**G**) *Sod2*, and (**H**) *Cat* on C2C12 myotubes incubated with oleate and palmitate (O/P) and with overexpression of *Ckmt2* compared with myotubes transfected with an empty vector and incubated with BSA or oleate and palmitate. Data are shown as means ± SEM (colored dots), and individual biological replicates are shown as gray dots paired by passage. $n = 6$ biological replicates ($n = 5$ in *Cat*). Each biological replicate is a different passage. Data were normalized to the empty vector incubated with a BSA control within each passage. qPCR was performed with technical duplicates. Statistical significance was determined by repeated-measurements one-way ANOVA followed by Tukey's post hoc test. $^{*}P < 0.05$; $^{**}P < 0.01$; $^{****}P < 0.0001$. (**I**) Ratio between activated $p38^{T180/Y182}$ MAPK and total p38 MAPK content in C2C12 myotubes shown on the left. Band intensity was normalized to Ponceau staining before calculating the ratio. A representative immunoblot is shown on the right. Data are shown as means ± SEM (colored dots), and individual biological replicates are shown as gray dots paired by passage. $n = 7$ biological replicates. Each biological replicate is a different passage. Data were normalized to the empty vector incubated with a BSA control within each passage. Statistical significance was determined by repeated-measurements one-way ANOVA followed by Tukey's post hoc test. $^{*}P < 0.05$; $^{**}P < 0.01$. (**J**) Relative palmitate oxidation capacity in myotubes overexpressing *Ckmt2* and incubated with oleate and palmitate compared with that in the BSA control. Data are shown as a Tukey's boxplot with individual dots paired by passage. $n = 6$ biological replicates. Each biological replicate is a different passage. Statistical significance was determined by repeated-measurements two-way ANOVA. (**K**) mRNA amounts normalized to control cells of genes involved in fatty acid handling, including *Sdc1*, (**L**) *Fas*, (**M**) *Sdc1*, and (**N**) *Ucp3*. Data are shown as means ± SEM (colored dots), and individual biological replicates are shown as gray dots paired by passage. $n = 6$ biological replicates ($n = 5$ in *Cat*). Each biological replicate is a different passage. Data were normalized to the empty vector incubated with a BSA control within each passage. qPCR was performed with technical duplicates. Statistical significance was determined by repeated-measurements one-way ANOVA followed by Tukey's post hoc test. $^{**}P < 0.01$; $^{***}P < 0.001$.

circulating creatine in plasma samples from men with type 2 diabetes, as well as reduced intramuscular phosphocreatine, recapitulating in vivo findings using phosphorus-31 magnetic resonance spectroscopy (*16*). Plasma creatine concentrations were inversely correlated with expression of the creatine transporter (*SLC6A8*) in skeletal muscle, reinforcing the major contribution of this tissue to the systemic

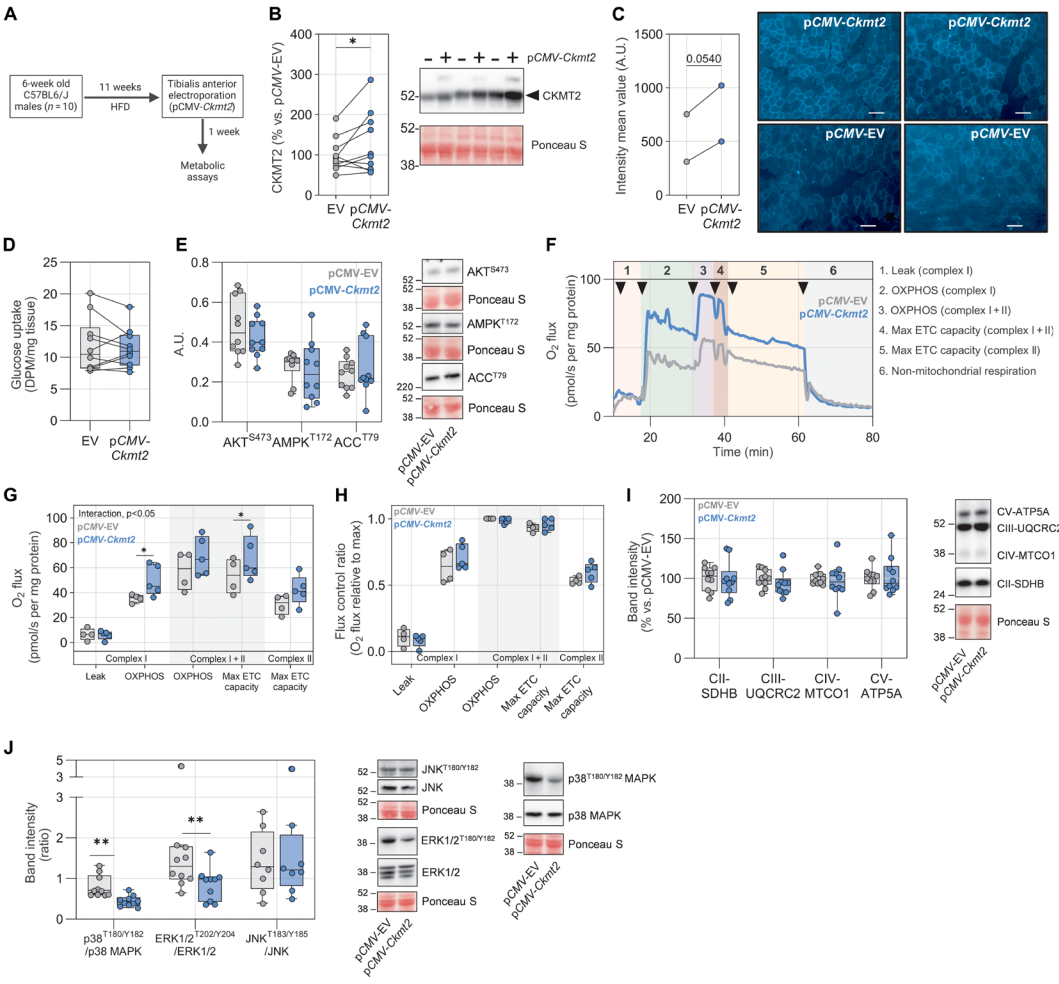

Fig. 5. In vivo overexpression of *Ckmt2* increases mitochondrial respiration and attenuates P38 activation in high-fat diet–fed mice. (**A**) Six-week-old C57BL/6 male mice were fed with a high-fat diet for 12 weeks. On the 11th week, the right tibialis anterior muscle was electroporated with a p*CMV-Ckmt2* vector to overexpress *Ckmt2*, whereas the left tibialis anterior muscle was electroporated with an empty vector (p*CMV*-EV) as control. Scheme of the experimental design created with BioRender.com. (**B**) Relative band intensity (left) and representative immunoblot (right) of CKMT2 in tibialis anterior muscle homogenates from mice described in (A). Band intensity was normalized to Ponceau staining and expressed as a percentage of the control leg. Data are shown as individual dots paired by mouse. $n = 10$ mice. Statistical significance was determined by one-tailed paired Student's t test. $^*P < 0.05$. (**C**) Fluorescence intensity (A.U.) (left) and representative immunofluorescence (right) of tibialis anterior muscle cryosections stained for CKMT2. Tibialis anterior muscles were dissected from mice described in (A). Data are shown as individual dots paired by mouse. $n = 2$ mice. Statistical significance was determined by one-tailed paired Student's t test. Scale bars, 100 μm. (**D**) Radiolabeled glucose uptake [disintegrations per minute (DPM) per milligram of tissue] in tibialis anterior muscles electroporated with an empty vector or with p*CMV-Ckmt2* as described in (A). Data are shown as a Tukey's box plot with individual dots paired by mouse. $n = 10$ mice. Statistical significance was determined by two-sided paired Student's t test. (**E**) Band densitometry (left) and representative blots (right) of AKT^{S473}, $AMPK^{T172}$, and ACC^{T79} from tibialis anterior muscle from mice described in (A). Band intensity was normalized to Ponceau staining. Data are shown as a Tukey's box plot. $n = 10$ mice. Statistical significance was determined by two-tailed paired Student's t test (AKT^{S473} and ACC^{T79}) or Wilcoxon matched-pairs signed-rank test ($AMPK^{T172}$). (**F**) Representative high-resolution respirometry assay in permeabilized tibialis anterior muscle fiber bundles. Arrowheads indicate sequential addition of glutamate-malate-pyruvate (ETC complex I substrates), ADP, succinate (complex II substrate), FCCP, rotenone, and antimycin A. The addition of these substrates led to the following respiratory states: (1) complex I leak respiration, (2) complex I oxidative phosphorylation (OXPHOS), (3) complex I + II OXPHOS, (4) complex I + II maximal ETC capacity, (5) complex II maximal ETC capacity, and (6) nonmitochondrial background respiration. (**G**) O_2 flux and (**H**) mitochondrial respiration normalized to maximal ETC capacity under different respiratory states [see (F)] in permeabilized fiber bundles from tibialis anterior muscles electroporated with an empty vector or with p*CMV-Ckmt2* as described in (A). Data are shown as a Tukey's box plot. $n = 4$ control mice, and $n = 5$ p*CMV-Ckmt2* mice. Statistical significance was determined by two-way ANOVA (mixed model) followed by Fisher's LSD test. $^*P < 0.05$. (**I**) Band densitometry (left) and representative immunoblots (right) of succinate dehydrogenase complex iron sulfur subunit B (SDHB) of complex II (CII), ubiquinol–cytochrome c reductase complex core protein 2 (UQCRC2) of complex III (CIII), cytochrome c oxidase subunit 1 (MTCO1) of complex IV (CIV), and ATP synthase F1 subunit α (ATP5A) of complex V (CV) in tibialis anterior muscle homogenates from mice described in (A). Band intensity was normalized to Ponceau staining and expressed as a percentage of the control leg. Data are shown as a Tukey's box plot. $n = 10$ mice. Statistical significance was determined by two-tailed paired Student's t test. (**J**) Ratio of phosphorylated $p38^{T180/Y182}$ MAPK, $ERK1/2^{T202/Y204}$, and $JNK^{T183/Y182}$ to nonphosphorylated p38 MAPK, ERK1/2, and JNK, respectively (left) and representative immunoblots (right) in tibialis anterior muscle homogenates from mice described in (A). Band intensity was normalized to Ponceau staining before calculating the phosphorylated-to-nonphosphorylated ratios. Data are shown as a Tukey's box plot. $n = 10$ mice in p38 MAPK and ERK1/2. $n = 8$ mice in JNK. Statistical significance was determined by a two-tailed Wilcoxon matched-pairs signed-rank test (p38 MAPK) or two-tailed paired Student's t test (ERK1/2 and JNK). $^{**}P < 0.01$.

circulating amounts of creatine. Conversely, in men with type 2 diabetes, skeletal muscle phosphocreatine content was reduced and associated with impaired glucose homeostasis. Nevertheless, the effects of creatine loading on glucose homeostasis are inconclusive, with some reports showing glucose-lowering effects (*17*, *18*), whereas others report increased skeletal muscle glycogen storage with no systemic effects on glucose homeostasis (*19*, *20*). Adding to this contention, creatine supplementation exacerbated glucose intolerance in a dexamethasone-induced muscle wasting rat model (*21*). These findings raise the question as to whether creatine metabolism alterations are a cause or a consequence of insulin resistance and impaired glucose tolerance. Here, we show that neither creatine supplementation

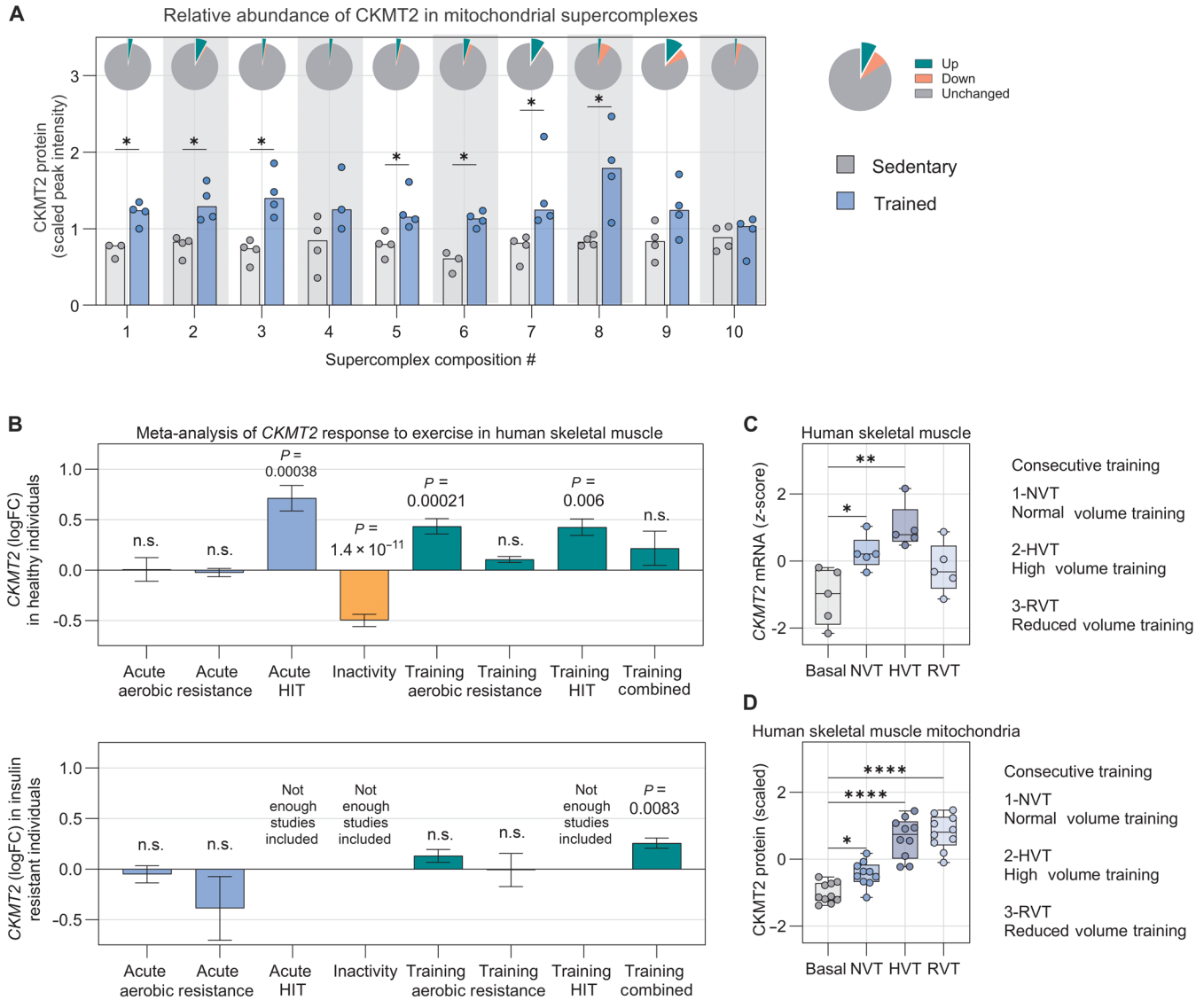

Fig. 6. CKMT2 expression is positively modulated by physical exercise. (**A**) Publicly available data (PXD016289) (*12*) were reanalyzed to examine the effects of exercise on CKMT2 protein abundance in isolated skeletal muscle mitochondria from sedentary mice and mice with free access to voluntary wheel running. The graph shows CKMT2 protein abundance in 10 different supercomplex compositions of the BN-PAGE gel. $n = 4$ mice (except for $n = 3$ in supercomplexes composition #1 and #6 in sedentary mice and supercomplex composition #4 in wheel running group). Statistical significance was determined by two-sided Student's t test. *$P < 0.05$. Pie charts at the top represent the proportion of significantly changed proteins. Significantly differentially expressed proteins between the sedentary and wheel running group were identified by the authors of the original study by combining the biological relevance (fold change) and the statistical significance (P value) (*12*). (**B**) Meta-analysis performed by the database MetaMEx (*13*) showing *CKMT2* mRNA amounts in skeletal muscle from healthy humans (top) and from individuals with insulin resistance (bottom) in response to different acute and training exercise protocols. The meta-analysis summary performed by MetaMEx was calculated using restricted maximum likelihood. The analysis was weighted using the sample size to adjust for studies with a small number of volunteers. (**C**) Publicly available raw data (PRJNA732106 and PXD026219) (*14*) were reanalyzed to examine the effects of physical exercise on CKMT2 in healthy human skeletal muscle mitochondria. RNA-seq data show *CKMT2* mRNA amounts in response to NVT, HVT, and RVT. Data are shown as a Tukey's box plot. $n = 5$ individuals. Statistical significance was determined by repeated-measurements one-way ANOVA followed by Dunnett's post hoc test. *$P < 0.05$; **$P < 0.01$. (**D**) Mitochondrial proteomics shows CKMT2 protein abundance in mitochondrial isolates after each training block (NVT, HVT, and RVT) compared with that at baseline [see (C)]. Data are shown as a Tukey's box plot. $n = 10$ individuals. Statistical significance was determined by repeated-measurements one-way ANOVA followed by Dunnett's post hoc test. *$P < 0.05$; ****$P < 0.0001$. n.s., not significant.

nor β-GPA–induced depletion of phosphocreatine modulates whole-body glucose metabolism in insulin-resistant mice. β-GPA is an antihyperglycemic compound that activates AMPK signaling and glucose transporter-4 translocation (*22*, *23*). Consistently, β-GPA treatment increased glucose uptake in oxidative and glycolytic skeletal muscle. However, β-GPA did not improve glucose tolerance or restored glycemia in insulin-resistant mice. Improvements in specific metabolic parameters in β-GPA–treated mice have also been reported without changes in glucose tolerance (*24*), suggesting that dose, treatment duration, and underlying metabolic health are

the critical factors influencing the metabolic outcomes associated with β-GPA (*22*, *24*, *25*). Creatine treatment increased mRNA of antioxidant genes in mouse skeletal muscle without functional alterations in glucose metabolism, suggesting that creatine supplementation is not deleterious to insulin action. Collectively, our data demonstrate that changes in creatine and phosphocreatine amounts are a consequence rather than a cause of insulin resistance.

Creatine is phosphorylated into phosphocreatine by creatine kinases. In skeletal muscle mitochondria, this reaction is catalyzed by CKMT2 (*6*). Concomitant with changes in creatine metabolites, we also noted lower expression of *CKMT2* in skeletal muscle from men with type 2 diabetes. CKMT2 protein has been found to be negatively enriched specifically in the mitochondrial proteome of patients with type 2 diabetes (*26*). Moreover, 8 weeks of high-fat–diet feeding, which rendered mice insulin resistant, also recapitulated the lower skeletal muscle *Ckmt2* expression. The reduced muscle phosphocreatine in patients with type 2 diabetes might be reflective of low CKMT2 expression. A reduced phosphocreatine recovery rate is a conventional surrogate marker of impaired mitochondrial function (*16*), which might partially reflect CKMT2 content in skeletal muscle. We show that silencing of *Ckmt2* in C2C12 myotubes reduced basal and maximal mitochondrial respiration, suggesting that CKMT2 abundance provides a molecular link between phosphocreatine and mitochondrial function. The depressed mitochondrial respiration in *Ckmt2*-silenced myotubes was accompanied by a moderate decrease in membrane potential. A hallmark of mitochondrial dysfunction is the loss of mitochondrial membrane potential, which can lead to reduced ATP generation (*27*), apoptotic signaling (*28*), and disrupted mitochondrial dynamics (*29*). Low membrane potential leads to the fragmentation of the mitochondrial network (*29*, *30*), consistent with increased presence of smaller mitochondria in *Ckmt2*-silenced C2C12 myotubes. Overall, the alterations in mitochondrial homeostasis after *Ckmt2* silencing ultimately reduced basal glucose oxidation. Thus, CKMT2 plays a critical role in maintaining mitochondrial function and integrity, thereby arising as a potential candidate for mitochondrial dysfunction in type 2 diabetes.

We found that lipid overload down-regulated *Ckmt2* expression, suggesting that intramuscular ectopic lipid accumulation contributes to the reduced abundance of CKMT2 in patients with type 2 diabetes. Creatine kinases and particularly CKMT2 are susceptible to oxidative damage (*31*, *32*), which is often associated with ectopic skeletal muscle fat (*33*). Thus, the lipid overload–induced reduction in CKMT2 likely plays a causal role in mitochondrial dysfunction and oxidative stress. We tested the hypothesis of whether overexpression of CKMT2 could, therefore, protect against lipid-induced metabolic stress. *Ckmt2* overexpression mitigated the lipid-induced activation of p38 MAPK, a stress- and ROS-responsive kinase implicated in the development of type 2 diabetes (*34*); up-regulated *Sod2* and *Cat* expression in palmitate-exposed C2C12 myotubes; and increased OXPHOS in muscle fibers. We propose that CKMT2 prevents oxidative stress by up-regulating antioxidant genes and promoting efficient mitochondrial respiration, thereby exerting a protection against metabolic stress associated with lipid overload. Moreover, mitochondrial creatine kinases prevent ROS production by recycling ADP in hyperglycemic conditions (*35*). Thus, the CKMT2 reduction in skeletal muscle from people with type 2 diabetes constitutes a potential molecular link between lipid overload–mediated impairments of mitochondrial function and metabolism.

Changes in CKMT2 content had profound effects on mitochondrial homeostasis and response to lipid-induced metabolic stress. The ex vivo respirometry assays were conducted in the absence of creatine, a potent modulator of mitochondrial respiration (*36*), indicating that increased mitochondrial respiration induced by CKMT2 overexpression was independent of changes in creatine-ADP stoichiometry. This result is compatible with CKMT1 depletion–induced mitochondrial depolarization, independent of phosphocreatine availability (*37*). Moreover, both CKMT1 and CKMT2 induce and stabilize contact sites between the inner and outer mitochondrial membrane by colocalizing with ANT and voltage-dependent anion channel (*38*–*40*). By analyzing publicly available data, we found that CKMT2 abundance is nonstoichiometrically enriched in skeletal muscle mitochondrial respiratory supercomplexes from trained mice (*12*). Although the functional role of mitochondrial supercomplexes remains controversial, a large number of studies suggest that these macromolecular structures could be involved in the integrity of ETC complexes, reduction of electron leakage, and ROS production (*41*). Hence, we hypothesize that reduction in CKMT2 leads to mitochondrial membrane destabilization, subsequently impairing mitochondrial function and homeostasis, contributing to disruptions in energy metabolism observed in metabolic disorders (fig. S4).

Altered mitochondrial homeostasis in skeletal muscle is regarded as a hallmark of type 2 diabetes and insulin resistance (*42*, *43*), although the direction of causality is a matter of intense debate (*44*–*46*). The effects of either reduced or increased CKMT2 as reported here were evident from experiments performed in the absence of insulin, thereby disassociating mitochondrial homeostasis from insulin signaling. Thus, the reduced CKMT2 expression in skeletal muscle from patients with type 2 diabetes likely contributes to impaired mitochondrial function, providing a plausible mechanism that disassociates mitochondrial capacity from insulin sensitivity. Conversely, our findings suggest that targeting CKMT2 might have therapeutic value to positively modulate mitochondrial function and metabolism. A meta-analysis of the transcriptomic response to exercise in human skeletal muscle revealed that, in healthy individuals, *CKMT2* is up-regulated by aerobic and high-intensity interval training and down-regulated by physical inactivity associated with bed rest and unloading (*13*). This response was severely dampened in individuals with insulin resistance, in which only a combination of aerobic and resistance training elicited changes in *CKMT2* expression. Moreover, physical exercise was able to not only up-regulate *CKMT2* mRNA but also increase and stabilize the abundance of CKMT2 protein in skeletal muscle mitochondria (*14*). The increase in CKMT2 was not stoichiometrically associated with the increase in mitochondrial content induced by training, suggesting that CKMT2 is specifically responsive to exercise. Thus, these results indicate that, whereas CKMT2 can be therapeutically targeted by physical exercise, there is a need for tailored training protocols to maximize the benefits of exercise in the type 2 diabetes population.

Last, it is worth noting that our study has several limitations. Only samples from male humans and rodents have been studied. Whereas epidemiological data show that increased plasma creatine is associated with the risk of type 2 diabetes in men but not women (*5*), our findings regarding the structural role of CKMT2 warrant further investigation in males and females, as well as in patient cohorts of different ancestries. Moreover, although our results show that CKMT2 regulates mitochondrial function independently of its kinase activity, the underlying structural mechanism needs to be

further explored. Last, the transcriptomic meta-analysis in individuals with insulin resistance was likely underpowered because of the limited number of exercise and transcriptomic studies in this population. Creatine metabolism is dependent on fiber-type distribution, which is different between humans and mice and thus a potential confounding factor. Because neither high-fat diet–induced insulin resistance in mice nor cultured human myotubes fully recapitulate human type 2 diabetes, additional confirmation in other models would further strengthen the conclusions presented here. Clinical studies in men and women aiming at up-regulating CKMT2 content would mitigate some of these limitations.

In conclusion, CKMT2 plays a key role in skeletal muscle mitochondrial homeostasis. *Ckmt2* reduction recapitulates key features of the skeletal muscle dysfunction in type 2 diabetes, including impaired mitochondrial function, increased ROS production, and reduced glucose metabolism. Conversely, *Ckmt2* overexpression increases OXPHOS and protects against lipid-induced metabolic stress. Collectively, we reveal a previously underappreciated role for CKMT2 in mitochondrial homeostasis, independent of creatine metabolism and insulin action. Thus, therapeutic strategies to increase CKMT2 expression, including tailored exercise training protocols, may be efficacious for treating metabolic disease.

METHODS

Study design

The study was designed to investigate the role of creatine metabolism in the development of type 2 diabetes. This goal was approached by measuring creatine metabolites and the expression of related genes in samples from men with type 2 diabetes [the study was approved by the regional ethical review board in Stockholm (EPN 2012/1047-31/2), and procedures were conducted according to the Declaration of Helsinki], by manipulating creatine amounts and the expression of *Ckmt2* in high-fat diet–fed mouse models [procedures were approved by the Stockholm North Animal Ethical Committee (N38/15)], and by determining the effects of *Ckmt2* expression on mitochondrial metabolism in C2C12 myotubes.

Cell culture experiments were conducted at minimum with three biological replicates and three technical replicates each. The number of animals in each group was initially calculated to measure at least moderate differences between the means of the experimental and control groups with a power of 80% and an α error probability of 5%. Mice with similar body weights were randomly assigned to the different groups. A preestablished end point of 20% of body weight loss from the beginning of the treatment was followed. Mouse experiments with creatine and creatine analogs were conducted in two different cohorts ($n = 5$ per group and cohort, final $n = 10$ per group). Only the analyses of electron microscopy and immunofluorescence images were performed in a blinded fashion.

Clinical data

Informed written consent was obtained from each participant. After clinical health screening and application of exclusion criteria (fig. S1A), 27 men with normal glucose tolerance and 25 men with type 2 diabetes were included in this study. Individuals with type 2 diabetes were treated with the following glucose-lowering drugs: metformin ($n = 20$; daily dose range, 500 to 3000 mg) and/or sulfonylurea [glibenclamide (glyburide), $n = 5$, 2 to 5 mg daily; glipizide, $n = 1$, 5 mg daily]. Glucose-lowering medication was taken by the individuals with type 2 diabetes after the skeletal muscle biopsy collection.

Individuals arrived at the clinic after an overnight 12-hour fast. Fasting blood samples were obtained. After subcutaneous application of local anesthesia (lidocaine hydrochloride, 5 mg/ml; Aspen Nordic), vastus lateralis biopsies were obtained using a conchotome (AgnTho's). Biopsies were immediately snap-frozen in liquid nitrogen and stored at −80°C. Total RNA microarray analysis was performed with the Affymetrix GeneChip Human Transcriptome Array 2.0 (Thermo Fisher Scientific). Metabolomic analysis was performed by Metabolon as described (*47*). Clinical characteristics of the individuals included in the metabolomic and transcriptomic analyses are shown in Tables 1 and 2.

Mouse studies

All mouse experiments were carried out in C57BL/6 male mice purchased from Charles River. Mice were housed in groups of four in ventilated cages with a 12-hour light/12-hour dark cycle in a temperature-controlled (20° to 24°C) environment with ad libitum access to food and water. All experimental procedures were approved by the Stockholm North Animal Ethical Committee (N38/15) and carried out according to the Karolinska Insitutet and ARRIVE (Animal Research: Reporting of In Vivo Experiments) animal care guidelines and European Union laws.

Creatine analog study

At 6 weeks of age, mice were fed either a standard chow diet ($n = 10$) (4% kcal from fat, R34; Lantmännen) or a 60% fat diet ($n = 30$) (Research Diets) for 8 weeks. At 12 weeks of age, mice were randomized to the treatment groups ($n = 10$ per group) on the basis of body weight and received daily intraperitoneal injections of PBS (20 ml/kg) or creatine (0.5 mg/kg body weight) for 14 days or β-GPA (0.4 mg/kg body weight) for 1 week (Fig. 2A). At the end of the treatment, body composition was assessed by magnetic resonance imaging (MRI) (EchoMRI-100, EchoMRI).

Intraperitoneal glucose tolerance test

One day before the last injection, mice were fasted for 4 hours, and glucose tolerance was determined. Glucose (2 g/kg body weight) was intraperitoneally administered, and blood glucose amounts were monitored for 2 hours with a glucometer (Contour XY, Bayer) using tail vein blood samples.

Electroporation-induced Ckmt2 overexpression experiments

At 6 weeks of age, mice were fed a 60% fat diet ($n = 15$) (Research Diets) for 11 weeks before the electroporation procedure. Briefly, mice were anesthetized with 2% isoflurane anesthesia, and both hind legs were shaved and cleaned with chlorhexidine. Hyaluronidase (30 μl of 1 U/μl) was injected intramuscularly in the tibialis anterior muscle, and mice returned to their home cage. After 2 hours, mice were anesthetized again with 2% isoflurane, and the tibialis anterior muscle of each leg was injected with either a p*CMV* plasmid encoding *Ckmt2* or an empty vector. Muscles were electroporated immediately after by delivering 220 V/cm in eight pulses of 20 ms using an ECM 830 electroporator (BTX Harvard Apparatus) (*48*).

Modified glucose tolerance test and in vivo glucose uptake

The effects of *Ckmt2* overexpression on skeletal muscle glucose transport were assessed with a modified glucose tolerance test. Briefly, a standard 2-hour OGTT was performed 7 days after electroporation. Fifteen minutes after oral gavage of glucose (3 g/kg body weight), mice were intraperitoneally injected with radioactive ^{3}H-2-deoxy-D-glucose (American Radiolabeled Chemicals, no. ART0103; 1 mCi/ml; specific

activity, 60 Ci/mmol). At the end of the test (120 min), mice were rapidly anesthetized, and the tibialis anterior muscles were immediately dissected and frozen in liquid nitrogen.

Tibialis anterior skeletal muscles were homogenized in 300 μl of phosphatidylinositol 3-kinase buffer [137 mM NaCl, 2.7 mM KCl, tris (pH 7.8), 1 mM $MgCl_2$, 1% Triton X-100, 10% glycerol, 10 mM NaF, and 1 mM EDTA], rotated at 4°C for 1 hour, and centrifuged at 13,000*g* for 10 min at 4°C. Thirty microliters of supernatants was analyzed by liquid scintillation counting to determine accumulation of ^{3}H-2-deoxy-D-glucose, and the remaining portion was stored at −80°C for immunoblot analysis.

Cell studies

Culture of the murine C2C12 muscle cell line

C2C12 myoblasts were cultivated in Dulbecco's modified Eagle's medium (DMEM) supplemented with 10% calf serum and containing 25 mM glucose, 4 mM L-glutamine, and 1 mM sodium pyruvate. Myogenic differentiation was induced in fully confluent cells by switching the calf serum in the growth medium for 2% horse serum. The experiments were performed after 5 days of differentiation.

Silencing and overexpression of Ckmt2

Cells were transfected with 200 nM siRNA targeting *Ckmt2* (si*Ckmt2*) or scrambled siRNA (siScr) as a control following the Lipofectamine RNAiMax manufacturer's instructions. For overexpression, cells were transfected with a p*CMV6*-entry vector containing the sequence of *Ckmt2* or an empty p*CMV6*-entry vector as a control following the Lipofectamine 3000 manufacturer's instructions. Transfection and differentiation medium switch was performed simultaneously.

Treatment with palmitate and oleate

Fatty acid–free BSA was solubilized in differentiation medium supplemented with 10 mM Hepes by agitation at 55°C for 15 min. Oleate and palmitate were added to a final concentration of 0.5 mM each and incubated at 55°C for 15 min. The solution was cooled down and filter sterilized (0.22 μm) before adding it to the cells. Control cells were treated with a vehicle consisting of 1% ethanol and 0.14% dimethyl sulfoxide in Hepes-supplemented differentiation medium. Myotubes were treated on the fifth day of differentiation for 18 hours.

RNA extraction, cDNA synthesis, and qPCR

RNA was extracted with TRIzol according to the manufacturer's instructions. RNA quality was assessed by spectrophotometry, and 1 μg was used as input for cDNA synthesis using the High-Capacity cDNA Reverse Transcription Kit. cDNA was diluted , and 10 ng was used in quantitative polymerase chain reaction (qPCR) with the indicated primer pairs (table S1). Relative mRNA quantification was calculated and normalized by RPL39 (cell studies) or hypoxanthine-guanine phosphoribosyltransferase (mouse studies) gene expression.

Western blotting

Skeletal muscle tissue was processed as described in the electroporation procedure. Cells were collected in radioimmunoprecipitation assay buffer (Thermo Fisher Scientific) and homogenized with the aid of a sonicator. Insoluble material was sedimented by centrifugation at 16,000*g*, and protein concentration in the supernatant was determined by Bradford assay. Laemmli buffer was added to the samples, and the proteins were resolved by gradient SDS–polyacrylamide gel electrophoresis (PAGE) (4 to 12%). Wet transfer was used to blot the proteins into polyvinylidene difluoride membranes, which were then stained with Ponceau S for normalization purposes and quality control. The membranes were blocked with 5% skimmed milk in TBS-T (Tris-buffered saline with Tween 20) [20 mM tris-HCl, 150 mM NaCl, and 0.02% (v/v) Tween 20 (pH 7.5)] for 1 hour. The membranes were incubated overnight with primary antibody as indicated and, after several washes, incubated for 1 hour with horseradish peroxidase (HRP)–conjugated secondary antibodies. Specific proteins were detected by enhanced chemiluminescence in an imager (Gel Doc XR System, Bio-Rad). Protein bands were quantified by densitometry using ImageLab software (Bio-Rad) and normalized by the Ponceau S densitometric volume of the respective gel lane. Catalogue numbers and RRIDs of used antibodies can be found in table S2.

ROS production assays

Cells were seeded in 96-well clear-bottom black plates and treated as indicated. Mitochondrial superoxide content was measured by MitoSOX probe fluorescence following the manufacturer's instructions. Briefly, cells were incubated with 5 μM MitoSOX in growth medium without serum for 30 min at 37°C and washed with PBS. Fluorescence at 510 nm/580 nm [excitation/emission (ex./em.)] was measured with a plate reader. Extracellular hydrogen peroxide content was measured with Amplex UltraRed Krebs-Henseleit Buffer in the presence of HRP (0.2 mU/ml) at 37°C. After an initial 10 min of incubation, fluorescence at 540 nm/590 nm (ex./em.) was measured every 15 min for 90 min, and the rate of fluorescence increase after background removal was calculated.

High-resolution respirometry

C2C12 myotubes

C2C12 myotubes were differentiated in a six-well plate. On the day of the experiment, cells were dissociated by adding 100 to 150 μl of trypsin and resuspended in 4 ml of warmed DMEM. Cells (1×10^6 to 2×10^6) were transferred to the respiration chambers. An aliquot of the cells was kept for later protein quantification and further normalization.

The effects of *Ckmt2* silencing on mitochondrial respiration were assessed by performing a phosphorylation control protocol with intact cells (*49*) in an Oxygraph-2k (Oroboros). Mitochondrial O_2 consumption was measured under basal conditions (ROUTINE, cells suspended in DMEM), under oligomycin treatment (2 μM ATP synthase inhibition; LEAK respiration), and under maximal respiration after FCCP titration in 1-μm steps (ETC capacity). These measurements were corrected by the passive, nonmitochondrial O_2 consumption obtained after the addition of the complex III inhibitor antimycin (2.5 μM) (ROX).

Skeletal muscle fiber bundles

Fiber bundles from electroporated tibialis skeletal muscle anterior were isolated and permeabilized with saponin (5 mg/ml) in ice-cold biopsy preservation solution BIOPS (10 mM Ca-EGTA buffer, 0.1 μM free calcium, 20 mM imidazole, 20 mM taurine, 50 mM K-MES, 0.5 mM dithiothreitol, 6.56 mM $MgCl_2$, 5.77 mM ATP, and 15 mM phosphocreatine) as described elsewhere (*50*). Fiber bundles (1.5 to 2.4 mg) were added to the respiratory chambers containing 2.2 ml of mitochondrial respiration medium MIR05 [110 mM sucrose, 20 mM Hepes, 20 mM taurine, 60 mM K-lactobionate, 3 mM $MgCl_2$, 10 mM KH_2PO_4, 0.5 mM EGTA, and BSA (1 g/liter) (pH 7.1)]. After adding the fibers to the respiration chamber, the chamber was closed, and the oxygen concentration was increased to ~400 μM and allowed to equilibrate before adding any substrates. Complex I leak respiration

was assessed by adding 2 mM malate, 10 mM pyruvate, and 10 mM glutamate. After O_2 consumption rates were stabilized, ADP was added to a final concentration of 5 mM, triggering complex I–driven OXPHOS. Complex II respiration was stimulated by adding 10 mM succinate, obtaining the OXPHOS capacity of complex I + complex II. ETC maximal capacity was determined by titrating FCCP in 0.5-μm steps. Complex II–linked ETC capacity was measured by inhibiting complex I with 0.5 μM rotenone. These measurements were corrected by ROX after adding 2.5 μM antimycin A. O_2 consumption rates were normalized to the fiber bundle weight added in each assay. Mitochondrial membrane integrity and damage were assessed by adding cytochrome c after measuring complex I respiration and observing no differences in O_2 consumption.

Citrate synthase activity assay

Cells were seeded in 96-well clear plates. Citrate synthase activity in C2C12 myotubes was measured with the Citrate Synthase Activity Assay Kit (MAK193, Sigma-Aldrich) and following the manufacturer's instructions. Absorbance at 412 nm was read every 5 min for 40 min.

Mitochondrial membrane potential

Cells were seeded in 96-well clear-bottom black plates. Mitochondrial membrane potential in C2C12 myotubes was measured in a fluorescence plate reader [535 nm/580 nm (ex./em, respectively)] with 50 nM TMRE and following the TMRE Mitochondrial Membrane Potential Assay Kit (ab113852, Abcam) according to the manufacturer's instructions.

Creatine measurements

Cells were transfected as indicated and were collected on the fifth day of differentiation. Creatine was quantified in cell lysates using the fluorometric mode of Creatine Assay (ab65339, Abcam) following the manufacturer's instructions. Absolute values were interpolated from a standard curve, and the data were normalized by protein content assessed by BCA (bicinchoninic acid) assay.

Electron microscopy

C2C12 myotubes were trypsinized and centrifuged, and pellets were fixed by immersion in 2.5% glutaraldehyde buffered in 0.1 M phosphate buffer (pH 7.4) at room temperature for 1 hour followed by storage at 4°C. Fixed cells were rinsed in 0.1 M phosphate buffer followed by postfixation in 2% osmium tetroxide in 0.1 M phosphate buffer (pH 7.4) at 4°C for 2 hours. After stepwise dehydration in ethanol and acetone, samples were resin infiltrated and lastly embedded in LX-112 (Ladd Research). Ultrathin sections (~80 to 100 nm) were prepared using an EM UC7 (Leica), transferred onto formvar stabilized slot grids, and contrasted with uranyl acetate followed by lead citrate. The grids were examined in a HT7700 transmission electron microscope (Hitachi High-Technologies) at 80 kV, and digital images were acquired using a 2kx2k Veleta CCD camera (Olympus Soft Imaging Solutions). Images were acquired and analyzed in a double-blinded manner. Mitochondria from three different passages of C2C12 myotubes were counted and measured with ImageJ. For statistical analysis, each individual mitochondrion was considered a biological replicate.

Immunofluorescence staining

Mouse tibialis anterior muscles were dissected and immediately frozen in liquid nitrogen–chilled isopentane and embedded in OCT (optimal cutting temperature) compound. Cross sections (10 μm) were obtained using a cryostat (Epredia CryoStar NX70). Before immunostaining, tissue slices were incubated with a blocking buffer (5% goat serum, 2% BSA, 0.1% sodium azide, and 0.1% Triton X-100 in PBS) at room temperature for 2 hours. Subsequently, slices were incubated overnight with CKMT2 antibody (ProteinTech) at a 1:400 dilution in the blocking buffer at 4°C. After incubation, the cryosections were washed and incubated with Alexa Fluor 488–conjugated secondary goat anti-rabbit antibodies at a 1:400 dilution (Invitrogen). Last, coverslips were mounted with UltraCruz mounting medium (sc-24941), and the samples were photographed using an Axio Vert A1 microscope (Zeiss). Whole-picture mean fluorescence intensity was measured with ZEN Lite microscopy software (version 3.9; Zeiss).

Public databases

Involvement of CKMT2 in mitochondrial supercomplexes

The potential involvement of CKMT2 in the formation of mitochondrial supercomplexes was analyzed by accessing a publicly available dataset (PXD016289) (*12*). In this study, the authors combined Blue native (BN)–PAGE and liquid chromatography–tandem mass spectrometry (LC-MS/MS) to assess the mitochondrial supercomplexomes in the triceps brachii muscles of sedentary and trained C57BL/6JBomTac female mice. Briefly, the authors isolated mitochondria from the triceps skeletal muscle ($n = 4$ per group) and ran equal amounts of mitochondrial protein in a BN-PAGE. Individual bands representing supercomplexes were excised and digested in-gel before being measured by LC-MS/MS. For the current analysis, we used the relative abundance of CKMT2 found in these supercomplexes bands before and after exercise training.

Effects of exercise on CKMT2 in human skeletal muscle

We used the MetaMEx database (*13*) to select studies of different types of acute and exercise training studies in metabolically healthy individuals and in individuals with insulin resistance, regardless of age, sex, or BMI, and conduct a meta-analysis on the skeletal muscle expression of *CKMT2* in response to exercise. The meta-analysis pipeline can be found on the MetaMEx website (https://metamex.serve.scilifelab.se/app/metamex).

To verify whether the observed changes in *CKMT2* mRNA were translated into CKMT2 mitochondrial protein, we used a publicly available database on the human mitochondrial proteome response to exercise (PXD026219) (*14*). In this study, young healthy individuals followed high-intensity interval training protocol consisting of 2 weeks of normal-volume training (NVT; 6 sessions), 3 weeks of high-volume training (HVT; 40 sessions), and 1 week of reduced-volume training (RVT; 6 sessions). Vastus lateralis biopsy samples were obtained at baseline and 72 hours after the last session of each training block. RNA-seq was performed in whole–skeletal muscle homogenates, whereas proteomics was conducted in skeletal muscle mitochondrial isolates.

Statistical analysis

Data derived from metabolomics are shown as median-scaled values for each metabolite. Gene expression signals from microarray datasets were log transformed. When possible, data are reported as Tukey's box plots with the median (line) and a 25 to 75% interquartile box. Whiskers reach the 25th and 75th percentiles ±1.5 times the interquartile distance. Results in tables are reported as means ± SEM. Data

normality was tested using the Shapiro-Wilk test, and parametric and nonparametric tests were used accordingly. Statistical significance between two groups with normally distributed data was determined by Student's *t* test, whereas a Mann-Whitney test and Wilcoxon matched-pairs signed-rank test were applied for unpaired and paired nonnormally distributed data, respectively. Welch's correction was applied when the SD was not assumed equal between groups. Statistical significance among three or more groups was determined by one- or two-way analysis of variance (ANOVA) according to the number of factors. ANOVAs were followed by Dunnett's post hoc test when comparing several groups only with a control group (i.e., when comparing several high-fat-diet groups against the only-chow group) and with Tukey's post hoc test when comparing all groups between them. A Kruskal-Wallis test followed by Dunn's multiple comparisons test was applied in instances where data were not normally distributed. Repeated measurement and mixed models were applied when measurements were matched or partially matched (i.e., different time points, same cell passages, or skeletal muscles from the same mouse). Data were analyzed using GraphPad Prism software (version 9.0.0; GraphPad software).

Supplementary Materials

The PDF file includes:
Materials and Methods
Figs. S1 to S4
Tables S1 to S3

Other Supplementary Material for this manuscript includes the following:
Data file S1
MDAR Reproducibility Checklist

REFERENCES AND NOTES

1. S. Bessman, P. Geiger, Transport of energy in muscle: The phosphorylcreatine shuttle. *Science* **211**, 448–452 (1981).
2. L. Ji, X. Zhao, B. Zhang, L. Kang, W. Song, B. Zhao, W. Xie, L. Chen, X. Hu, Slc6a8-mediated creatine uptake and accumulation reprogram macrophage polarization via regulating cytokine responses. *Immunity* **51**, 272–284.e7 (2019).
3. L. Kazak, P. Cohen, Creatine metabolism: Energy homeostasis, immunity and cancer biology. *Nat. Rev. Endocrinol.* **16**, 421–436 (2020).
4. S. Maqdasy, S. Lecoutre, G. Renzi, S. Frendo-Cumbo, D. Rizo-Roca, T. Moritz, M. Juvany, O. Hodek, H. Gao, M. Couchet, M. Witting, A. Kerr, M. O. Bergo, R. P. Choudhury, M. Aouadi, J. R. Zierath, A. Krook, N. Mejhert, M. Ryden, Impaired phosphocreatine metabolism in white adipocytes promotes inflammation. *Nat. Metab.* **4**, 190–202 (2022).
5. A. Post, D. Groothof, J. C. Schutten, J. L. Flores-Guerrero, J. C. Swarte, R. M. Douwes, I. P. Kema, R. A. de Boer, E. Garcia, M. A. Connelly, T. Wallimann, R. P. F. Dullaart, C. F. M. Franssen, S. J. L. Bakker, Plasma creatine and incident type 2 diabetes in a general population-based cohort: The PREVEND study. *Clin. Endocrinol. (Oxf)* **94**, 563–574 (2021).
6. T. Wallimann, M. Wyss, D. Brdiczka, K. Nicolay, H. M. Eppenberger, Intracellular compartmentation, structure and function of creatine kinase isoenzymes in tissues with high and fluctuating energy demands: The 'phosphocreatine circuit' for cellular energy homeostasis. *Biochem. J.* **281**, 21–40 (1992).
7. K. Fritz-Wolf, T. Schnyder, T. Wallimann, W. Kabsch, Structure of mitochondrial creatine kinase. *Nature* **381**, 341–345 (1996).
8. U. Schlattner, L. Kay, M. Tokarska-Schlattner, "Mitochondrial proteolipid complexes of creatine kinase" in *Membrane Protein Complexes: Structure and Function*, Subcellular Biochemistry series, J. R. Harris, E. J. Boekema, Ed. (Springer, 2018), vol. 87, pp. 365–408.
9. L. Kay, K. Nicolay, B. Wieringa, V. Saks, T. Wallimann, Direct evidence for the control of mitochondrial respiration by mitochondrial creatine kinase in oxidative muscle cells in situ. *J. Biol. Chem.* **275**, 6937–6944 (2000).
10. R. A. DeFronzo, E. Jacot, E. Jequier, E. Maeder, J. Wahren, J. P. Felber, The effect of insulin on the disposal of intravenous glucose. Results from indirect calorimetry and hepatic and femoral venous catheterization. *Diabetes* **30**, 1000–1007 (1981).
11. R. J. Snow, R. M. Murphy, Factors influencing creatine loading into human skeletal muscle. *Exerc. Sport Sci. Rev.* **31**, 154–158 (2003).
12. A. Gonzalez-Franquesa, B. Stocks, S. Chubanava, H. B. Hattel, R. Moreno-Justicia, L. Peijs, J. T. Treebak, J. R. Zierath, A. S. Deshmukh, Mass-spectrometry-based proteomics reveals mitochondrial supercomplexome plasticity. *Cell Rep.* **35**, 109180 (2021).
13. N. J. Pillon, B. M. Gabriel, L. Dollet, J. A. B. Smith, L. Sardon Puig, J. Botella, D. J. Bishop, A. Krook, J. R. Zierath, Transcriptomic profiling of skeletal muscle adaptations to exercise and inactivity. *Nat. Commun.* **11**, 470 (2020).
14. C. Granata, N. J. Caruana, J. Botella, N. A. Jamnick, K. Huynh, J. Kuang, H. A. Janssen, B. Reljic, N. A. Mellett, A. Laskowski, T. L. Stait, A. E. Frazier, M. T. Coughlan, P. J. Meikle, D. R. Thorburn, D. A. Stroud, D. J. Bishop, High-intensity training induces non-stoichiometric changes in the mitochondrial proteome of human skeletal muscle without reorganisation of respiratory chain content. *Nat. Commun.* **12**, 7056 (2021).
15. J. Vangipurapu, L. Fernandes Silva, T. Kuulasmaa, U. Smith, M. Laakso, Microbiota-related metabolites and the risk of type 2 diabetes. *Diabetes Care* **43**, 1319–1325 (2020).
16. E. M. Ripley, G. D. Clarke, V. Hamidi, R. A. Martinez, F. D. Settles, C. Solis, S. Deng, M. Abdul-Ghani, D. Tripathy, R. A. DeFronzo, Reduced skeletal muscle phosphocreatine concentration in type 2 diabetic patients: A quantitative image-based phosphorus-31 MR spectroscopy study. *Am. J. Physiol. Endocrinol. Metab.* **315**, E229–E239 (2018).
17. B. Rocic, N. B. Bajuk, P. Rocic, D. S. Weber, J. Boras, M. V. Lovrencic, Comparison of antihyperglycemic effects of creatine and metformin in type II diabetic patients. *Clin. Invest. Med.* **32**, E322 (2009).
18. K. Rooney, J. Bryson, J. Phuyal, G. Denyer, I. Caterson, C. Thompson, Creatine supplementation alters insulin secretion and glucose homeostasis in vivo. *Metabolism* **51**, 518–522 (2002).
19. L. J. van Loon, R. Murphy, A. M. Oosterlaar, D. Cameron-Smith, M. Hargreaves, A. J. Wagenmakers, R. Snow, Creatine supplementation increases glycogen storage but not GLUT-4 expression in human skeletal muscle. *Clin. Sci. (Lond.)* **106**, 99–106 (2004).
20. B. O. Eijnde, E. A. Richter, J. C. Henquin, B. Kiens, P. Hespel, Effect of creatine supplementation on creatine and glycogen content in rat skeletal muscle. *Acta Physiol. Scand.* **171**, 169–176 (2001).
21. H. Nicastro, B. Gualano, W. M. de Moraes, V. de Salles Painelli, C. R. da Luz, A. dos Santos Costa, F. de Salvi Guimaraes, A. Medeiros, P. C. Brum, A. H. Lancha Jr., Effects of creatine supplementation on muscle wasting and glucose homeostasis in rats treated with dexamethasone. *Amino Acids* **42**, 1695–1701 (2012).
22. M. D. Meglasson, J. M. Wilson, J. H. Yu, D. D. Robinson, B. M. Wyse, C. J. de Souza, Antihyperglycemic action of guanidinoalkanoic acids: 3-Guanidinopropionic acid ameliorates hyperglycemia in diabetic KKAy and C57BL6Job/ob mice and increases glucose disappearance in rhesus monkeys. *J. Pharmacol. Exp. Ther.* **266**, 1454–1462 (1993).
23. K. E. Pandke, K. L. Mullen, L. A. Snook, A. Bonen, D. J. Dyck, Decreasing intramuscular phosphagen content simultaneously increases plasma membrane FAT/CD36 and GLUT4 transporter abundance. *Am. J. Physiol. Regul. Integr. Comp. Physiol.* **295**, R806–R813 (2008).
24. J. D. Dorigatti, K. M. Thyne, B. C. Ginsburg, A. B. Salmon, Beta-guanidinopropionic acid has age-specific effects on markers of health and function in mice. *Geroscience* **43**, 1497–1511 (2021).
25. I. Oudman, J. F. Clark, L. M. Brewster, The effect of the creatine analogue beta-guanidinopropionic acid on energy metabolism: A systematic review. *PLOS ONE* **8**, e52879 (2013).
26. S. Chae, S. J. Kim, Y. Do Koo, J. H. Lee, H. Kim, B. Y. Ahn, Y. C. Ha, Y. H. Kim, M. G. Jang, K. H. Koo, S. H. Choi, S. Lim, Y. J. Park, H. C. Jang, D. Hwang, S. W. Lee, K. S. Park, A mitochondrial proteome profile indicative of type 2 diabetes mellitus in skeletal muscles. *Exp. Mol. Med.* **50**, 1–14 (2018).
27. L. D. Zorova, V. A. Popkov, E. Y. Plotnikov, D. N. Silachev, I. B. Pevzner, S. S. Jankauskas, V. A. Babenko, S. D. Zorov, A. V. Balakireva, M. Juhaszova, S. J. Sollott, D. B. Zorov, Mitochondrial membrane potential. *Anal. Biochem.* **552**, 50–59 (2018).
28. G. Kroemer, P. Petit, N. Zamzami, J. L. Vayssiere, B. Mignotte, The biochemistry of programmed cell death. *FASEB J.* **9**, 1277–1287 (1995).
29. Y. Miyazono, S. Hirashima, N. Ishihara, J. Kusukawa, K. I. Nakamura, K. Ohta, Uncoupled mitochondria quickly shorten along their long axis to form indented spheroids, instead of rings, in a fission-independent manner. *Sci. Rep.* **8**, 350 (2018).
30. E. Jones, N. Gaytan, I. Garcia, A. Herrera, M. Ramos, D. Agarwala, M. Rana, W. Innis-Whitehouse, E. Schuenzel, R. Gilkerson, A threshold of transmembrane potential is required for mitochondrial dynamic balance mediated by DRP1 and OMA1. *Cell. Mol. Life Sci.* **74**, 1347–1363 (2017).
31. S. Wendt, U. Schlattner, T. Wallimann, Differential effects of peroxynitrite on human mitochondrial creatine kinase isoenzymes. Inactivation, octamer destabilization, and identification of involved residues. *J. Biol. Chem.* **278**, 1125–1130 (2003).
32. E. A. Konorev, N. Hogg, B. Kalyanaraman, Rapid and irreversible inhibition of creatine kinase by peroxynitrite. *FEBS Lett.* **427**, 171–174 (1998).
33. P. P. Sfyri, N. Y. Yuldasheva, A. Tzimou, N. Giallourou, V. Crispi, A. Aburima, P. Beltran-Alvarez, K. Patel, V. Mougios, J. R. Swann, M. T. Kearney, A. Matsakas, Attenuation of oxidative stress-induced lesions in skeletal muscle in a mouse model of

obesity-independent hyperlipidaemia and atherosclerosis through the inhibition of Nox2 activity. *Free Radic. Biol. Med.* **129**, 504–519 (2018).
34. E. Bengal, S. Aviram, T. Hayek, p38 MAPK in glucose metabolism of skeletal muscle: Beneficial or harmful? *Int. J. Mol. Sci.* **21**, 6480 (2020).
35. L. E. Meyer, L. B. Machado, A. P. Santiago, W. S. da-Silva, F. G. De Felice, O. Holub, M. F. Oliveira, A. Galina, Mitochondrial creatine kinase activity prevents reactive oxygen species generation: Antioxidant role of mitochondrial kinase-dependent ADP re-cycling activity. *J. Biol. Chem.* **281**, 37361–37371 (2006).
36. B. Walsh, M. Tonkonogi, K. Soderlund, E. Hultman, V. Saks, K. Sahlin, The role of phosphorylcreatine and creatine in the regulation of mitochondrial respiration in human skeletal muscle. *J. Physiol.* **537**, 971–978 (2001).
37. C. Datler, E. Pazarentzos, A. L. Mahul-Mellier, W. Chaisaklert, M. S. Hwang, F. Osborne, S. Grimm, CKMT1 regulates the mitochondrial permeability transition pore in a process that provides evidence for alternative forms of the complex. *J. Cell Sci.* **127**, 1816–1828 (2014).
38. O. Speer, N. Back, T. Buerklen, D. Brdiczka, A. Koretsky, T. Wallimann, O. Eriksson, Octameric mitochondrial creatine kinase induces and stabilizes contact sites between the inner and outer membrane. *Biochem. J.* **385**, 445–450 (2005).
39. U. Schlattner, M. Dolder, T. Wallimann, M. Tokarska-Schlattner, Mitochondrial creatine kinase and mitochondrial outer membrane porin show a direct interaction that is modulated by calcium. *J. Biol. Chem.* **276**, 48027–48030 (2001).
40. U. Schlattner, M. Tokarska-Schlattner, T. Wallimann, Mitochondrial creatine kinase in human health and disease. *Biochim. Biophys. Acta* **1762**, 164–180 (2006).
41. S. Javadov, S. Jang, X. R. Chapa-Dubocq, Z. Khuchua, A. K. Camara, Mitochondrial respiratory supercomplexes in mammalian cells: Structural versus functional role. *J. Mol. Med. (Berl)* **99**, 57–73 (2021).
42. D. E. Kelley, J. He, E. V. Menshikova, V. B. Ritov, Dysfunction of mitochondria in human skeletal muscle in type 2 diabetes. *Diabetes* **51**, 2944–2950 (2002).
43. J. A. Kim, Y. Wei, J. R. Sowers, Role of mitochondrial dysfunction in insulin resistance. *Circ. Res.* **102**, 401–414 (2008).
44. S. Bajpeyi, M. Pasarica, C. Moro, K. Conley, S. Jubrias, O. Sereda, D. H. Burk, Z. Zhang, A. Gupta, L. Kjems, S. R. Smith, Skeletal muscle mitochondrial capacity and insulin resistance in type 2 diabetes. *J. Clin. Endocrinol. Metab.* **96**, 1160–1168 (2011).
45. B. H. Goodpaster, L. M. Sparks, Metabolic flexibility in health and disease. *Cell Metab.* **25**, 1027–1036 (2017).
46. S. Bajpeyi, M. Pasarica, K. E. Conley, B. R. Newcomer, S. A. Jubrias, C. Gamboa, K. Murray, O. Sereda, L. M. Sparks, S. R. Smith, Pioglitazone-induced improvements in insulin sensitivity occur without concomitant changes in muscle mitochondrial function. *Metabolism* **69**, 24–32 (2017).
47. A. M. Evans, C. D. DeHaven, T. Barrett, M. Mitchell, E. Milgram, Integrated, nontargeted ultrahigh performance liquid chromatography/electrospray ionization tandem mass spectrometry platform for the identification and relative quantification of the small-molecule complement of biological systems. *Anal. Chem.* **81**, 6656–6667 (2009).
48. S. S. Kulkarni, H. K. Karlsson, F. Szekeres, A. V. Chibalin, A. Krook, J. R. Zierath, Suppression of 5′-nucleotidase enzymes promotes AMP-activated protein kinase (AMPK) phosphorylation and metabolism in human and mouse skeletal muscle. *J. Biol. Chem.* **286**, 34567–34574 (2011).
49. E. Gnaiger, K. Renner-Sattler, High-resolution respirometry and phosphorylation control protocol with intact cells: ROUTINE, LEAK, ETS, ROX. *Mitochondrial Physiol. Netw.* **8**, 8 (2014).
50. A. V. Kuznetsov, V. Veksler, F. N. Gellerich, V. Saks, R. Margreiter, W. S. Kunz, Analysis of mitochondrial function in situ in permeabilized muscle fibers, tissues and cells. *Nat. Protoc.* **3**, 965–976 (2008).

Acknowledgments: We acknowledge A.-M. Pettersson for expertise and support in conducting animal experiments. Electron microscopy data were collected at the Karolinska Institutet 3D-EM facility (https://ki.se/cmb/3d-em). Figure schematics were created with BioRender.com where indicated in the legends. **Funding:** This study was supported by a Novo Nordisk postdoctoral fellowship at Karolinska Institutet (to D.R.-R.), a Wenner-Gren Foundation postdoctoral fellowship and a São Paulo Research Foundation (FAPESP) research internship abroad grant 2021/07411-2 (to D.S.P.S.F.G.), and a Karolinska Institutet doctoral fellowship (to L.A.P.). The research was supported by an EFSD/Lilly Young Investigator Research Award Programme grant (to D.R.-R.), a Margareta af Ugglas Foundation grant (to M.R.), the Swedish Research Council (to J.R.Z., M.R., and A.K.), ERC-SyG SPHERES grant 856404 (to M.R.), Novo Nordisk Foundation - MeRIAD consortium grant 0064142 (to M.R. and A.K.) and a project grant (to J.R.Z.), the Swedish Diabetes Foundation (to M.R., J.R.Z., and A.K.), CIMED (to M.R.), and the Knut and Alice Wallenberg Foundation (including Wallenberg Clinical Scholar) (to M.R., E.N., J.R.Z., and A.K.). **Author contributions:** D.R.-R., M.R., J.R.Z., and A.K. conceived the project. D.R.-R. and D.S.P.S.F.G. designed the experiments. D.R.-R., D.S.P.S.F.G., L.A.P., and S.M. performed studies in mice. D.R.-R., L.A.P., and A.V.C. performed ex vivo skeletal muscle glucose uptake experiments. D.R.-R., D.S.P.S.F.G., and N.D.L. performed in vitro assays. D.S.P.S.F.G. amplified p*CMV* plasmids, transfected cells, and prepared histological sections. E.N. collected clinical samples. D.R.-R., M.R., J.R.Z., and A.K. provided funding. D.R.-R. analyzed the data, made the figures, and wrote the original draft of the paper, which was reviewed and edited by J.R.Z. and A.K. All coauthors reviewed the final version of the draft. **Competing interests:** The authors declare that they have no competing interests. **Data and materials availability:** All data associated with this study are present in the paper or the Supplementary Materials. The study used commercially available antibodies and reagents, with details provided in tables S1 to S3. Publicly available datasets used in the study can be found in the ProteomeXchange Consortium PRIDE repository (accession codes PXD016289 and PXD026219) and in NCBI BioProject (accession code PRJNA732106).

Submitted 28 January 2024
Accepted 16 September 2024
Published 9 October 2024
10.1126/scitranslmed.ado3022